Torsti Alku

Quantification of APROS' physical model uncertainties in the context of the PREMIUM benchmark

School of Science

Master´s thesis submitted in partial fulfillment of the requirements for the degree of Master of Science in Technology in the Degree Programme in Engineering Physics and Mathematics.
Espoo 13.12.2013

Thesis supervisor:

Prof. Rainer Salomaa

Thesis instructor:

Lic.Sc. (Tech.) Joona Kurki

Aalto University
School of Science

AALTO UNIVERSITY
SCHOOL OF SCIENCE

ABSTRACT OF THE
MASTER'S THESIS

Author: Torsti Alku

Title: Quantification of APROS' physical model uncertainties in the context of the PREMIUM benchmark

Date: 13.12.2013 Language: English Number of pages: 7+59

Degree programme: Engineering Physics and Mathematics

Major: Advanced Energy Systems Minor: Economics (University of Helsinki)

Chair (Code): Advanced Energy Systems (Tfy-56)

Supervisor: Prof. Rainer Salomaa Instructor: Lic.Sc. (Tech.) Joona Kurki

Quantifying uncertainties by using so called Best-Estimate Plus Uncertainty methods is a growing trend in nuclear power plant safety research. One way for these BEPU methods to account for them is by propagation of input uncertainties through code calculations. For this purpose it is necessary to know the uncertainties of the physical models that are used by codes to close the conservation equations in addition to other sources.

In this master's thesis uncertainties of the thermal hydraulic system code APROS are investigated. Specifically, the physical models dealing with phenomena taking place in reactor core reflooding scenarios are examined.

Three methods proposed in the international PREMIUM benchmark for the quantification of the uncertainties are reviewed. Two of them, the FFTBM and CIRCE methods, are applied to a paradigm application of the FRIGG loop experiments with APROS. With confidence gained through the application, the methods are then put into use with six FEBA reflooding experiments within the scope of the phase III of the PREMIUM benchmark.

The results of the application, probability distribution functions (PDFs) of multipliers of the physical models, are further on used to calculate uncertainty bounds for output parameters of a PERICLES 2D reflooding experiment. It can be seen from the PDFs themselves as well as from the PERICLES 2D results that the uncertainties related to the physical models used by APROS are very large.

Due to biases in the physical models of APROS, as well as problems with the process of application of the FFTBM and CIRCE methods, the ranges of the uncertainties are so wide that the usability of the PDFs is limited. Still, the work performed in this master's thesis serves as a good basis both for further code development as well as BEPU studies with APROS.

Keywords: Nuclear safety research, Thermal hydraulic system codes, Physical models, APROS, BEPU, Probability distribution function, PREMIUM benchmark, FEBA, PERICLES, FFTBM, CIRCE

AALTO-YLIOPISTO
PERUSTIETEIDEN KORKEAKOULU

DIPLOMITYÖN
TIIVISTELMÄ

Tekijä: Torsti Alku

Työn nimi: APROS:n fysikaalisten mallien epävarmuuksien määrittäminen PREMIUM vertailulaskun kontekstissa

Päivämäärä: 13.12.2013 Kieli: Englanti Sivumäärä: 7+59

Tutkinto-ohjelma: Teknillinen fysiikka ja matematiikka

Pääaine: Energiatieteet Sivuaine: Kansantaloustiede (Helsingin Yliopisto)

Opetusyksikkö (ent. professuuri) (Koodi): Energiatieteet (Tfy-56)

Valvoja: Prof. Rainer Salomaa Ohjaaja: TkL Joona Kurki

Epävarmuuksien määrittäminen niin kutsuttujen Best-Estimate Plus Uncertainty -menetelmien avulla on kasvava trendi ydinvoimalaitosten turvallisuustutkimuksessa. Eräs tapa, jolla BEPU-menetelmät voivat ottaa ne huomioon, on syötteiden epävarmuuksien johtaminen koodien laskujen läpi. Tätä tarkoitusta varten on tiedettävä koodien säilymislait sulkevien fysikaalisten mallien epävarmuudet muiden lähteiden lisäksi.

Tässä diplomityössä tutkitaan termohydraulisen systeemikoodi APROS:n epävarmuuksia. Erityisesti tarkastelun alla ovat ne fysikaaliset mallit, jotka vaikuttavat reaktorisydämen tulvittamistilanteessa esiintyviin ilmiöihin.

Työssä katselmoidaan kolme kansainvälisessä PREMIUM-vertailulaskussa ehdotettua menetelmää epävarmuuksien määrittämiseen. Kahta niistä, FFTBM ja CIRCE -menetelmiä, käytetään APROS:n kanssa yksinkertaiseen esimerkkitapaukseen, FRIGG-kokeisiin. Menetelmien käyttämisestä kertyneen luottamuksen turvin niitä sovelletaan FEBA-tulvittamiskokeisiin PREMIUM-vertailulaskun vaiheen III puitteissa.

FEBA-sovelluksen tuloksia, fysikaalisten mallien todennäköisyysjakaumia, käytetään myöhemmin yhden PERICLES 2D -tulvittamiskokeen ulostuloparametrien ylä- ja alarajojen laskemiseen. Todennäköisyysjakaumista itsestään, sekä PERICLES 2D -tuloksista nähdään, että APROS:n käyttämiin fysikaalisiin malleihin liittyvät epävarmuudet ovat suuria.

APROS:n fysikaalisissa malleissa esiintyvien poikkeamien, sekä FFTBM ja CIRCE -menetelmien käyttämiseen liittyvän prosessin ongelmien takia epävarmuuksien vaihtelualueet ovat niin suuria, että niiden käytettävyys on rajoitettua. Silti, tässä diplomityössä esitelty analyysi toimii hyvänä pohjana niin koodin jatkokehitykselle, kuin BEPU-jatkotutkimuksille APROS:n kanssa.

Avainsanat: Ydinturvallisuustutkimus, Termohydrauliset systeemikoodit, Fysikaaliset mallit, APROS, BEPU, Todennäköisyysjakauma, PREMIUM benchmark, FEBA, PERICLES, FFTBM, CIRCE

Preface

The work presented in this master's thesis has been funded by the Finnish Research Program on Nuclear Power Plant Safety 2011 – 2014 (SAFIR2014). Instructions on the FFTBM method presented in this master's thesis was provided by the University of Pisa, and instructions and software tools for the use of CIRCE by CEA. Knowledge gained at the 2012 Seminar and training on Scaling, UNcertainty and 3D COuPled code calculations in nuclear technology (3D S.UN.COP) has also been of great use during the course of the writing of this master's thesis.

I wish to thank my professor Rainer Salomaa for his supervision of the thesis as well as his support during the course of my studies. Furthermore, I wish to thank my instructor Joona Kurki for the immense help, instruction, mentoring and support he has given me while I have been writing the thesis; for answering all my questions ranging from the lightest grammatical point to the fundamentals of the physics under investigation. Without his guidance this thesis would not have come to be.

I also wish to forward my gratitude to Markku Hänninen, Jukka Ylijoki and Ismo Karppinen for sharing their knowledge of APROS, thermal hydraulics and for general support in my work. My boss, Eija-Karita Puska, I wish to thank for giving me the opportunity to carry out this research and for providing moral support through all of it.

Finally I wish to say that I am extremely grateful to my wife-to-be, Laura Rojas (to-be Alku), for supporting me during this entire time I have been working on the thesis; for having the patience to listen to my complaints and offer guidance; for sharing this burden with me; for having fun with me; for loving me; and in the end for proof reading the thesis and pointing out the smallest of errors.

Otaniemi, December 13, 2013

Torsti O. Alku

Contents

Abbreviations

AA	Average Amplitude
ASAP	Adjoint Sensitivity Analysis Procedure
BEMUSE	Best-Estimate Methods – Uncertainty and Sensitivity Evaluation
BEPU	Best-Estimate Plus Uncertainty
CEA	Commissariat à l'énergie atomique et aux énergies alternatives
CFD	Computational Fluid Dynamics
CFR	Code of Federal Regulations
CIAU	Code with the capability of Internal Assessment of Uncertainty
CIRCE	Calculation of the Uncertainties Related to the Elementary Correlations
CSNI	Committee on the Safety of Nuclear Installations
ECME	Expectation-Conditional Maximisation Either
EM	Expectation Maximisation
FEBA	Flooding Experiments with Blocked Array
FFTBM	Methodology using the Fast Fourier Transform Based Method
GAA	Global Average Amplitude
GRS	Gesellschaft für Anlagen- und Reaktorsicherheit
KIT	Karlsruhe Institute of Technology
LBLOCA	Large Break Loss-Of-Coolant Accident
LHS	Latin Hypercube Sampling
LOFT	Loss Of Fluid Test facility
LSTF	Large Scale Test Facility
NEA	Nuclear Energy Agency
NPP	Nuclear Power Plant
OECD	Organisation for Economic Co-operation and Development
PDF	Probability Density Function

PREMIUM	Post-BEMUSE REflood Models Input Uncertainty Methods
RMS	Root Mean Square
SAFIR2014	Finnish Research Program on Nuclear Power Plant Safety 2011 – 2014
SBLOCA	Small Break Loss-Of-Coolant Accident
UMAE	Uncertainty Method based on Accuracy Extrapolation
UMS	Uncertainty Methods Study
WF	Weighted Frequency

1 Introduction

Computer codes are used extensively in nuclear safety research. The codes handle problems in different areas of interest and levels of accuracy. Thermal-hydraulic codes deal with the motion, thermal balance and phase changes of fluids. Computational Fluid Dynamics (CFD) codes strive to recreate actual physical phenomena accurately, whereas the focus of thermal-hydraulic system codes is to be able to model entire systems all the way up to full nuclear power plants.

Modern thermal-hydraulic system codes balance between the aspiration to reproduce physical phenomena as realistically as possible and conserving used computer time. To achieve this the codes use conservation equations for liquid and gas phases, which are discretized in volume and time. Coupled with physical models – built from empirical correlations developed from experimental data – the codes are able to model complete thermal-hydraulic systems.

The obvious limitation of the system approach is that the properties of the medium are averaged over the discretization cells, which results in loss of data and phenomena smaller than the cell size. Additionally, the correlations used to build the physical models, especially historically, have been derived from small scale steady state experiments, whereas they are applied to full scale reactor transients.

The development of thermal-hydraulic system codes begun in the 1970's with extensive experimental programs designed to create the physical models for the codes. Previously nuclear safety analysis codes were based on a conservative approach due to the limitations of the prevailing knowledge and computational capacity. The codes were based on conservative input values as well as a conservative view on the physics of the situation under investigation. The idea was that, because the real state of a system could not be determined, it was better to try to determine the worst possible situation and base reactor design limits on that. [1, 2, 3]

With the introduction of realistic codes the concept of best-estimate was coined. As the name suggests, the codes were to provide the best possible estimate of the behavior of the system under current knowledge. Still, the simulated results were only estimations since uncertainties in the code and the input values remained. A best-estimate code used in conjunction with conservative input values could be used to produce conservative estimates of the results. In fact this was and still is the approach used for licensing in many countries.

The main benefit of moving from using conservative codes with conservative values to best-estimate codes with conservative values was that the conservative codes could, in some cases, produce misleading and even unphysical results. The events of a transient could be reproduced in wrong order or be totally omitted. Also, there was no way of quantifying the conservatism of the calculations, which the best-estimate codes allowed.

The next step after the emergence of best-estimate codes was to take the uncertainties caused by various sources into account in calculation of the results. In the United States the part of the Code of Federal Regulations dealing with nuclear power (10 CFR 50) and its Appendix K, which define safety limits and criteria of nuclear power plant design and operation, did not allow the use of best-estimate

codes until a 1989 revision, which stated that uncertainties had to be taken into account.

Several different approaches have been pursued to estimate the uncertainties of the output of thermal hydraulic system codes. Eight different so called Best-Estimate Plus Uncertainty (BEPU) methods were presented at the OECD/NEA/ CSNI Workshop on Uncertainty Analysis Methods in 1994 [4]. The Workshop was followed by the Uncertainty Methods Study (UMS) [5] from 1994 to 1998, where five of the methods were compared to each other through a practical application. The uncertainty methods were applied to a 5% cold leg Small Break Loss-Of-Coolant Accident (SBLOCA) experiment performed in the Japanese Large Scale Test Facility (LSTF).

The Best-Estimate Methods – Uncertainty and Sensitivity Evaluation (BEMUSE) program (2004-2011) [6] followed the UMS with the number of methods having been reduced to two. These are the Code with the capability of Internal Assessment of Uncertainty (CIAU) method, the successor to Uncertainty Method based on Accuracy Extrapolation (UMAE), developed by the University of Pisa, and a statistical method developed by the German research institute Gesellschaft für Anlagen- und Reaktorsicherheit (GRS). The former focuses on the propagation of output errors, or extrapolation of code accuracy, whereas the latter involves the propagation of input errors, or input uncertainty, through the code runs.

The CIAU method [7] is based on identifying plant states which are defined by several output parameters, for example pressure, power and mass inventory. For each state the accuracy of the code is derived by comparing the results of a multitude of experiments to respective simulations. When applying the method to a new case, one best-estimate simulation is run and the plant state is simply determined at each moment of the simulation. Then the accuracy of the code in those states defines the uncertainty bands of the results.

The statistical method, often referred to as the GRS method [8] is based on assigning a Probability Density Function (PDF) to each uncertain input parameter and running a certain number of code runs, while randomly varying all parameters within these PDFs. The results of the runs are then put together creating upper and lower limits for the output parameters. The number of runs required depends on the desired tolerance limits of the results based on order statistics, specifically the Wilks' formula [9].

Whereas the UMS was a pilot study into the general applicability of the uncertainty methods, the BEMUSE program focused on refining the application of the methods and creating further understanding of their use. The program consisted of applying the uncertainty methods to two different cases. First they were applied to an experiment of a Large Break Loss-Of-Coolant Accident (LBLOCA) performed at the Idaho National Laboratory Loss Of Fluid Test (LOFT) facility and second to an LBLOCA simulated with a generic computer model of the Zion Nuclear Power Plant (NPP) located in Illinois, United States.

Nine out of ten participants in the BEMUSE used the GRS method due to its relative ease of application leaving only the University of Pisa to use their own CIAU method. For this reason the focus of the results of the program turned more

to the investigation of the use of the GRS method. In that respect a particular importance was noted in the specification of the PDFs. The conclusion was that either reduction of the use of expert judgement, or formalization of the process of using expert judgement, was required to produce more reliable results.

The largest issues with assigning the PDFs were found to be with parameters dealing with the physical models of the code, also known as constitutive equations; even users of the same code could assign very different PDFs for the variation of their models [6]. On the other hand the determination of the PDFs of the basic input parameters dealing with physical quantities of the experiment was found to be easier and consensus could readily be found. In fact a list of parameters with ranges of variation was given by the organizers for the NPP application phase in the program.

According to the findings of the BEMUSE program the BEPU methods are ready and mature enough for use in safety studies and licensing of NPP's. Nevertheless it was recognized that future research is required. Especially in the case of the statistical method the uncertainties related to the code models are critically important to the results of the application of the method. As a consequence, their definition has been put under research in the Post-BEMUSE REflood Models Input Uncertainty Methods (PREMIUM) benchmark endorsed by OECD/NEA/CSNI. VTT Technical Research Centre of Finland participates in the benchmark with the system code APROS developed in partnership with Fortum.

The PREMIUM benchmark was started in 2011 and has, as of this writing, proceeded to its fourth and final phase. The idea of the benchmark is to define methods for the quantification of the uncertainties of the physical models of the codes and apply them to the models that are deemed influential. Phase I consisted of introduction of some of the methods proposed for the quantification. In phase II each participant identified the influential parameters in the case of a reflooding experiment and the purpose of phase III was to use the previously defined methods to quantify the uncertainties. Phase IV serves as a confirmation or verification of the defined PDFs when the participants perform a blind calculation of another experiment using the previously defined PDFs.

In this master's thesis different sources of uncertainties in thermal hydraulic system code calculations are considered and some of the methods used in the benchmark for the quantification of the physical model uncertainties are presented. Their applicability for use with APROS is investigated with through a paradigm application. Also the previously performed task of identifying the influential parameters in the case of a reflooding experiment is referred to, while the work carried out to produce VTT's contribution to phase III of the benchmark is presented. Additionally, Phase IV of the benchmark is introduced and preliminary results are analyzed. Finally a more general view of the matter at hand in the perspective of VTT is given.

2 Input uncertainty methods

2.1 Sources of uncertainty

Uncertainties in thermal hydraulic code calculations arise from five different types of sources as defined in [10]. These types may be described as *representation uncertainty*, *scaling issue*, *plant uncertainty*, *user effect* and *code uncertainty*. All of the sources of uncertainty are also related to each other.

The uncertainty related to representation refers to how real volumes are portrayed by the computer model, or input deck[1]. The portrayal of the volumes is also known as nodalization and the process of setting it up includes compromises between calculation speed and accuracy, as well as taking into account the limitations of the used thermal hydraulic code. Representation uncertainty can be mitigated by forming clear guidelines for making the nodalization, but it is also difficult to take into account in BEPU analysis.

The scaling issue arises from the fact that experiments are in general performed in small scale compared to nuclear power plants. Thus all code development and their use is based on small scale phenomena and whether they can be generalized to full scale is not always clear. The scaling issue and how to solve it is an ongoing area of discussion within the thermal hydraulic system code community. The best way to approach it is to validate the codes on several scales with similar or counterpart tests. As such the uncertainty related to the scaling issue can not be taken into account in BEPU analysis.

Plant uncertainty is the uncertainty of the physical properties and dimensions of the facility under consideration, which are used as boundary and initial conditions in simulations. These include, for example, the uncertainty of the instruments used for measuring different parameters. Mitigating plant uncertainty is not tied to the computer codes and thus is not part of BEPU analysis. These uncertainties can be taken into account in the analysis, though, through uncertainties of boundary and initial conditions, as well as through uncertainties of the experimental results, which are compared to the simulation results.

User effects have been recognized to affect results significantly. They were witnessed for example in the Uncertainty Methods Study [5]. These effects depend on the way a code user applies the code to a simulation task; what assumptions they make and how they put them into effect. User effects are lessened by creating rigorous guidelines for all of the phases in a BEPU analysis, but the uncertainty that may still remain can not be taken into account because it is not quantifiable.

Code uncertainty stems from several sources dealing with the calculation of the thermal hydraulic solution. These include the uncertainty of the numerical solutions of the conservation laws that form the basis of a thermal hydraulic code, as well as that of the empirical correlations or consitutive equations, which describe different physical processes. Uncertainty is also brought by special models built to handle

[1]Input deck refers to all the data or variables that is input to a computer code to calculate output data. Historically input decks consisted of several punch cards, or pieces of paper with holes in them, which were inserted into the computers.

specific complex situations eg. steam separation. All code uncertainties the source of which can be varied can be taken into account in BEPU analysis. For example a multiplier can be assigned to the constitutive equations, which allows their variation.

Essentially the uncertainties that can be taken into account with BEPU analysis are the plant uncertainties and the codes' constitutive equation uncertainties. During the course of the BEMUSE program it was acknowledged that plant uncertainties are known or can be agreed upon with relative ease. The consitutive equations, on the other hand, pose more challenges. Different codes use different equations and different relations between them. Also, in complex systems the connections between particular equations – and the physical phenomena they describe – and particular output responses are not always clear. Thus the determination of the uncertainties of the constitutive equations is non-trivial.

The PREMIUM benchmark focuses on the quantification of the uncertainties of the consitutive equations. Several different organizations take part in the benchmark using several different codes. Some of the organizations have previously developed methods to quantify the uncertainties with their codes and some methods are being developed during the benchmark. In the following sections three of the most promising methods are presented and two of them applied to a simple case study.

2.2 FFTBM

The *Methodology for characterizing the range of input uncertainty parameters by the use of the FFTBM* is being developed by the University of Pisa. Due to its ongoing development it has not been published yet and is used in this master's thesis as it is presented below.

The methodology uses the Fast Fourier Transform Based Method, which is a part of the Uncertainty Method based on Accuracy Extrapolation. Within the scope of the UMAE methodology the FFTBM is used primarily to detect the accuracy of code calculations compared to experimental calculations [4]. The benefit of using Fourier transform is to move from time domain to frequency domain without loss of information and to characterize the accuracy with two single values, the Average Amplitude (AA) and Weighted Frequency (WF).

Within the scope of the characterization of input uncertainty, the accuracy of several calculations using different values for a particular input parameter is compared to the accuracy of a reference calculation. The AA and WF are calculated for several outputs for a given calculation. To describe the accuracy of the whole calculation a quadratic weighted average is calculated for AA. The weights used for the different outputs depend on the respective experimental accuracy and the relevance of the outputs for safety.

The result of the previous steps is the difference of the accuracy of an input parameter variation calculation to the accuracy of the reference calculation, referred to as Global Average Amplitude (GAA). The variation range for an input parameter is then defined by specifying an acceptability threshold for the GAA. A uniform distribution is applied for the variation range due to the lack of knowledge about its true form.

2.2.1 Mathematical formulation

An error or difference function is required to calculate the accuracy of a code calculation. The simplest way is to deduct the experimental values from the calculated values giving the difference function the form

$$\Delta F(t) = F_{\text{calc}}(t) - F_{\text{exp}}(t), \tag{1}$$

where "calc" and "exp" refer to calculated and experimental results, respectively, and t defines the point in time.

To use the Fourier transform on discrete functions the Fast Fourier Transform algorithm is used, which requires the amount of values to be a power of two. To achieve this both experimental and calculated values need to be interpolated. Sufficient amount of points should be used to avoid loss of information.

The two values, which can be used to characterize the accuracy, the average amplitude AA and weighted frequency WF, are defined respectively as

$$\text{AA} = \frac{\sum_{n=0}^{2^m} |\widetilde{\Delta F}(f_n)|}{\sum_{n=0}^{2^m} |\widetilde{F}_{\text{exp}}(f_n)|}, \tag{2}$$

$$\text{WF} = \frac{\sum_{n=0}^{2^m} |\widetilde{\Delta F}(f_n)| \cdot f_n}{\sum_{n=0}^{2^m} |\widetilde{\Delta F}(f_n)|}, \tag{3}$$

where the tilde refers to the Fourier transform, m defines the number of values as the power of two and f_n are the transformed frequencies. The AA can be seen as a measure of average relative error comparing to the experimental calculation, whereas the WF describes which frequency causes the largest part of the error.

The results of using the FFT algorithm are $m/2$ negative frequencies, the 0 Hz frequency and $m/2-1$ positive frequencies. These frequencies are symmetric around the 0 Hz frequency (except for the $m/2$th negative frequency) and can thus be folded to the positive side. When the amplitudes are also normalized by dividing with the number of points the result is a series of amplitudes for a real cosine series, which could be used to recreate the original signal. The amount of frequencies is diminished to $m/2+1$, whereas the amplitudes of the frequencies between 0 Hz and the maximum frequency are multiplied by two.

The folding and normalization are important, when introducing a *cut frequency* above which the amplitudes are discarded, when calculating the AA and WF. The cut frequency depends on the sampling rate of the original signals and should not be higher than half of the sampling frequency. This is due to avoiding spurious information as directed by the sampling theorem [11].

To describe the accuracy of a whole calculation the average amplitude and weighted frequency are calculated for multiple outputs. A quadratic weighted average is then calculated of the amplitudes and this is divided by the quadratic weighted

average of a reference calculation. Finally, the so called global average amplitude $\mathrm{AA}_G^{*,\mathrm{IP}}$ takes the form

$$\mathrm{AA}_G^{*,\mathrm{IP}} = \sqrt{\frac{\sum_{i=1}^{N}(\mathrm{AA}_{R_i}^{*,\mathrm{IP}} \cdot w_{f_i})^2}{\sum_{i=1}^{N}(\mathrm{AA}_{R_i}^{\mathrm{REF}} \cdot w_{f_i})^2}}, \tag{4}$$

where $*$ refers to the sensitivity – or variation – calculation of the input parameter under consideration, "REF" to the reference calculation, R_i is the ith output parameter and w_{f_i} is the weight of the ith output parameter. The weights are defined during the general development of the method by considering several separate effect test facility experiments, and is an ongoing process.

To quantify the variation ranges of an input parameter several sensitivity calculations should be performed and the $\mathrm{AA}_G^{*,\mathrm{IP}}$ calculated for them. A threshold value $T1$ is then defined under which the fractional difference to the reference calculation should be.

$$\mathrm{AA}_G^{*,\mathrm{IP}} - 1 < T1. \tag{5}$$

In addition, no output parameter average amplitude within the sensitivity runs should exceed a certain threshold. This threshold has been set during the development of the FFTBM method as

$$\mathrm{AA}_{R_i}^{*,\mathrm{IP}} < 0.1. \tag{6}$$

2.2.2 Use of the method

The workflow of the methodology for characterizing the range of input uncertainty parameters by the use of the FFTBM can be summarized for a single uncertain input parameter as follows:

1. Run reference case
2. Select output parameters
3. Derive all the $\mathrm{AA}_{R_i}^{\mathrm{REF}}$
4. Select uncertain input parameter
5. Run sensitivity cases for the input parameter
6. Derive all the $\mathrm{AA}_{R_i}^{*,\mathrm{IP}}$ (one per output parameter) and the $\mathrm{AA}_G^{*,\mathrm{IP}}$ (one per sensitivity calculation)
7. Define threshold value and identify the variation range
8. Discard input parameter, if it is not relevant

2.3 CIRCE

Calcul des Incertitudes Relatives aux Corrélations Élementaires (English: Calculation of the Uncertainties Related to the Elementary Correlations) [12] is a method developed in the 1990's by the French research organization CEA (Commissariat à l'énergie atomique et aux énergies alternatives) to define the uncertainties of the constitutive equations of their in-house code CATHARE. It comes accompanied with a computer program, which has been designed to take CATHARE output as its input, but any other thermal hydraulic code output can be used if formatted properly.

The CIRCE method uses derivatives of code output in respect to a limited number of input parameters defined at pre-set points to optimize the outputs in respect to experimental results by variation of the inputs. In essence, the method solves a simplified problem describing the thermal-hydraulic system code and input deck. The products are the most likely values for the defined set of input parameters in the form of Probability Distribution Functions (PDF). The PDFs consist of a center value, which has been shifted by a bias, and a standard deviation.

To achieve its purpose CIRCE uses the Expectation-Conditional Maximization Either (ECME) algorithm, which is an extension of the Expectation Maximization (EM) algorithm. However the CIRCE method was developed separately from the ECME algorithm based on the EM algorithm. EM and ECME are based on the principle of maximum likelihood and the iterative Bayes' theorem. All these concepts are common statistical tools.

Several hypotheses are made, when using CIRCE, which are required by the statistical tools used. The two most important ones are that a linear (or log-linear) relationship is assumed between the input and output parameters, and the input parameters are assumed to be normally (or log-normally) distributed. Three additional requirements apply for the usage of CIRCE:

- experimental uncertainties – if taken into consideration – need to be independent of the difference between code calculation results and real values in the experiment
- the difference between code best-estimate, or reference calculation and experimental results needs to be globally higher than experimental uncertainties (otherwise CIRCE results are single values instead of distributions)
- the output points need to be independent of each other; addition of dependent points does not add information

Additionally, the input parameters are most often assumed to be independent of each other in applications of the CIRCE method, but this is not required.

2.3.1 Mathematical formulation

The purpose of the CIRCE method is to produce a bias vector $\boldsymbol{b}$ and an affiliated covariance matrix $\boldsymbol{C}$, which describe the possible values of the input parameter

vector $\boldsymbol{\alpha}$. They are formulated as

$$\boldsymbol{b} = \begin{pmatrix} b_1 \\ b_2 \\ \vdots \\ b_N \end{pmatrix}, \boldsymbol{C} = \begin{pmatrix} \sigma_1^2 & 0 & \cdots & 0 \\ 0 & \sigma_2^2 & \cdots & 0 \\ \vdots & \vdots & \ddots & \vdots \\ 0 & 0 & \cdots & \sigma_N^2 \end{pmatrix}, \boldsymbol{\alpha} = \begin{pmatrix} \alpha_1 \\ \alpha_2 \\ \vdots \\ \alpha_N \end{pmatrix},$$

where N defines the amount of input parameters under consideration and σ_i, $i = 1, \ldots, N$ is the standard deviation of the respective probability density function with center value at $\alpha_i + b_i$. N is normally between 2 and 4, and should not be much higher to minimize the complexity of the solution and possible spurious results.

The CIRCE application sets the nominal values for the parameters α_i as 0. Thus a change of variable is required, when CIRCE is applied to code input parameters, which in the case of constitutive equations are multipliers. The function f performing the change needs to fill two conditions: $f(0) = 1$ and $f'(0) = 1$. The first condition defines the nominal value of the multiplier and the second guarantees that the derivatives found for the multipliers can be used directly.

Two useful functions fill the requirements of the change of variable: $p_i = 1 + \alpha_i$ and $p_i = exp(\alpha_i)$, where p_i is the ith input parameter. These functions also abide by the hypoteses of linearity, or log-linearity, required by the proper functioning of CIRCE.

The input of CIRCE is similarly in vector and matrix form. The demanded inputs are the experimental and best-estimated reference calculation results $\boldsymbol{R}^{\text{exp}}$ and $\boldsymbol{R}^{\text{calc}}$, as well as a matrix of the derivatives of the outputs in respect to the input parameters $\boldsymbol{\partial R}$:

$$\boldsymbol{R}^{\text{exp}} = \begin{pmatrix} (R_1^{\text{exp}}) \\ (R_2^{\text{exp}}) \\ \vdots \\ (R_M^{\text{exp}}) \end{pmatrix}, \boldsymbol{R}^{\text{calc}} = \begin{pmatrix} (R_1^{\text{calc}}) \\ (R_2^{\text{calc}}) \\ \vdots \\ (R_M^{\text{calc}}) \end{pmatrix}, \boldsymbol{\partial R} = \begin{pmatrix} \frac{\partial R_1}{\partial \alpha_1} & \frac{\partial R_1}{\partial \alpha_2} & \cdots & \frac{\partial R_1}{\partial \alpha_N} \\ \frac{\partial R_2}{\partial \alpha_1} & \frac{\partial R_2}{\partial \alpha_2} & \cdots & \frac{\partial R_2}{\partial \alpha_N} \\ \vdots & \vdots & \ddots & \vdots \\ \frac{\partial R_M}{\partial \alpha_1} & \frac{\partial R_M}{\partial \alpha_2} & \cdots & \frac{\partial R_M}{\partial \alpha_N} \end{pmatrix},$$

where M is the number of output points chosen for the application and R_j^{exp} and R_j^{calc} respectively the experimental and calculated values of the jth point, $j = 1, \ldots, M$. Usually M is several tens up to over a hundred. The algorithm used by CIRCE can also take experimental accuracies into account, if desired, input as standard deviations, but for simplicity they are not included in the following formulas.

When analyzing simple models, it is possible to use the Adjoint Sensitivity Analysis Procedure (ASAP) [13] to deduce the derivatives $\frac{\partial R_j}{\partial \alpha_i}$. A tool for this calculation has been built to accompany CATHARE, but it can only be used with 1D models which do not include reflooding or fuel. Practically in all thermal hydraulics calculations the derivatives thus have to be deduced from sensitivity calculations by varying a single parameter a small amount at a time. Special care has to be taken to make sure the derivatives so acquired are representative.

To calculate the bias vector $\boldsymbol{b}$ and covariance matrix $\boldsymbol{C}$ the principle of maximum likelihood and Bayes' theorem are used consecutively, while holding the other one

of the variables constant. After an initial guess at their values they are updated through an iterative process until they converge. The full procedure is explained by references [12] and [14]. The following explains the first step of the algorithm.

If the bias $\boldsymbol{b}$ is set constant to equal zero, the covariance matrix $\boldsymbol{C}$ can be estimated with the help of the principle of maximum likelihood as

$$\widehat{C} = \frac{1}{M} \sum_{j=1}^{M} \boldsymbol{\alpha}_j \boldsymbol{\alpha}_j^{\mathrm{T}}, \tag{7}$$

where $\widehat{\ }$ denotes the estimation and $\boldsymbol{\alpha}_j$ is the input parameter vector corresponding to the point j. The vector $\boldsymbol{\alpha}_j$ has been adjusted so that the calculated value R_j^{calc} would match the experimental value R_j^{exp} at point j based on the derivatives of the input parameters. A linear model is used to define a correlation for the difference between the calculated and experimental value as follows

$$(R_j^{\mathrm{exp}} - R_j^{\mathrm{calc}}) = \frac{\boldsymbol{\partial R_j}}{\boldsymbol{\partial \alpha}}^{\mathrm{T}} \boldsymbol{\alpha}_j. \tag{8}$$

Taking variance from both sides gives the following

$$\mathrm{var}(R_j^{\mathrm{exp}} - R_j^{\mathrm{calc}}) = \mathrm{var}\left(\frac{\boldsymbol{\partial R_j}}{\boldsymbol{\partial \alpha}}^{\mathrm{T}} \boldsymbol{\alpha}_j \right) = \frac{\boldsymbol{\partial R_j}}{\boldsymbol{\partial \alpha}}^{\mathrm{T}} \boldsymbol{C} \frac{\boldsymbol{\partial R_j}}{\boldsymbol{\partial \alpha}}. \tag{9}$$

Equation (8) cannot be solved explicitly, because the left side is a scalar and $\boldsymbol{\alpha}_j$ is a vector. Assuming that the $\boldsymbol{\alpha}_j$ vectors, as well as the experimental to calculation differences, follow a normal distribution allows the use of the Bayes' theorem. It is applied to calculate an estimation for the mean vectors $\overline{\boldsymbol{\alpha}}_j$ and covariance matrices $\boldsymbol{C}_j$ of each $\boldsymbol{\alpha}_j$ vector using a guess of an *a priori* covariance matrix $\boldsymbol{C}^{(i-1)}$. The equations for the mean and covariance are

$$\overline{\boldsymbol{\alpha}}_j = \boldsymbol{C}^{(i-1)} \times \frac{\boldsymbol{\partial R_j}}{\boldsymbol{\partial \alpha}} \times \frac{R_j^{\mathrm{exp}} - R_j^{\mathrm{calc}}}{\frac{\boldsymbol{\partial R_j}}{\boldsymbol{\partial \alpha}}^{\mathrm{T}} \boldsymbol{C}^{(i-1)} \frac{\boldsymbol{\partial R_j}}{\boldsymbol{\partial \alpha}}}, \tag{10}$$

$$\boldsymbol{C}_j = \boldsymbol{C}^{(i-1)} - \frac{\boldsymbol{C}^{(i-1)} \frac{\boldsymbol{\partial R_j}}{\boldsymbol{\partial \alpha}} \frac{\boldsymbol{\partial R_j}}{\boldsymbol{\partial \alpha}}^{\mathrm{T}} \boldsymbol{C}^{(i-1)}}{\frac{\boldsymbol{\partial R_j}}{\boldsymbol{\partial \alpha}}^{\mathrm{T}} \boldsymbol{C}^{(i-1)} \frac{\boldsymbol{\partial R_j}}{\boldsymbol{\partial \alpha}}}. \tag{11}$$

To calculate an adjusted, or *a posteriori* covariance matrix the principle of maximum likelihood is used, as shown in equation (7), where $\boldsymbol{C}^{(i)} = \widehat{\boldsymbol{C}}$. Since Bayes' theorem provides only mean and covariance matrices of the input parameter vectors $\boldsymbol{\alpha}_j$ an expectation value is used, calculated as

$$E(\boldsymbol{\alpha}_j \boldsymbol{\alpha}_j^{\mathrm{T}}) = \overline{\boldsymbol{\alpha}}_j \overline{\boldsymbol{\alpha}}_j^{\mathrm{T}} + \boldsymbol{C}_j. \tag{12}$$

Inserting equations (10) and (11) into equation (12) and further on to equation (7) provides the following formula for the updated covariance matrix $\boldsymbol{C}^{(i)}$:

$$\boldsymbol{C}^{(i)} = \boldsymbol{C}^{(i-1)} + \frac{1}{M}\sum_{j=1}^{M} \frac{\boldsymbol{C}^{(i-1)}\dfrac{\boldsymbol{\partial R_j}}{\boldsymbol{\partial \alpha}}\dfrac{\boldsymbol{\partial R_j}}{\boldsymbol{\partial \alpha}}^{\mathrm{T}}\boldsymbol{C}^{(i-1)}}{\dfrac{\boldsymbol{\partial R_j}}{\boldsymbol{\partial \alpha}}^{\mathrm{T}}\boldsymbol{C}^{(i-1)}\dfrac{\boldsymbol{\partial R_j}}{\boldsymbol{\partial \alpha}}} \left(\frac{(R_j^{\mathrm{exp}} - R_j^{\mathrm{calc}})^2}{\dfrac{\boldsymbol{\partial R_j}}{\boldsymbol{\partial \alpha}}^{\mathrm{T}}\boldsymbol{C}^{(i-1)}\dfrac{\boldsymbol{\partial R_j}}{\boldsymbol{\partial \alpha}}} - 1 \right) \tag{13}$$

After the covariance matrix has been calculated, the same procedure is applied to calculate the bias vector $\boldsymbol{b}$. The equations involved are modified accordingly and the previously acquired covariance matrix is used in the calculations as a constant. After both have been calculated the process is repeated updating the *a priori* covariance matrix and bias vector with the *a posteriori* matrix and vector of the previous iteration until convergence is reached.

CIRCE also provides a mean to distinguish output points, which are not fit for the analysis. They include points, where the calculated reference value is far off from the experimental value compared to the effect the chosen input parameters have on the point. This can be due to high absolute value of the difference between experimental and calculated value, or low sensitivity of the point to chosen input parameters. In any case, the reason for the point not fitting needs to be figured out before disregarding any point.

To distinguish unfit output points CIRCE calculates the separation between the difference of the experimental and calculated values to the one approximated by CIRCE with the resulting bias vector (see equation (8)). Because both are expected to follow a normal distribution, also their separation should follow normal distribution. Thus, when the separation is divided by variance the results should follow a standardized normal distribution. Then, depending on the amount of points, abnormally high absolute values of the so called residuals can be pointed out. The formula for the residuals r_j is:

$$r_j = \frac{(R_j^{\mathrm{exp}} - R_j^{\mathrm{calc}}) - \dfrac{\boldsymbol{\partial R_j}}{\boldsymbol{\partial \alpha}}^{T}\boldsymbol{b}}{\dfrac{\boldsymbol{\partial R_j}}{\boldsymbol{\partial \alpha}}^{T}\boldsymbol{C}\dfrac{\boldsymbol{\partial R_j}}{\boldsymbol{\partial \alpha}}} \tag{14}$$

2.3.2 Use of the method

The use of the CIRCE method contains several steps, some of which require expert judgment and thus need to be carried out with great care. The steps of the application of CIRCE can be summarized as follows:

1. Select uncertain input parameters
2. Run sensitivity and best-estimate runs
3. Choose output points

4. Derive all the $\frac{\partial R_j}{\partial \alpha_i}$ (per j output points and i input parameters)
5. Create CIRCE input file and run CIRCE
6. Check the residuals and remove unfit output points, if required
7. Run sensitivity calculations to determine that hypothesis of linearity is met and whether linear or log-linear formulation is better
8. Transform the bias results, b_i, to input parameter distributions, p_i
9. Check that new best-estimate runs with biases produce better results
10. Check that for example 93 randomly varied runs envelop about 95% of experimental output points (BEPU analysis)

The CIRCE method can be used iteratively so, that after running new best-estimate runs the calculated results in the procedure are replaced by the new results. The derivatives also need to be transformed depending on the formulation of the linear relation. In the case of linear formulation the derivatives may be used as is, but in the case of log-linear formulation the derivatives need to be multiplied by the value of the input parameter bias, b_i.

After an iteration run the bias is added to the previously calculated ones. With every iteration the absolute value of the new bias should get smaller in order for convergence to be possible. Usually only around four iterations are required until the absolute value of the bias is small enough to assume convergence. Since the method is not exact, only an approximate convergence is required.

The result of the application of CIRCE is a normal or log-normal distribution, which may be cut at some distance from the mean value. Two-sigma distance can be utilized, as it provides 95% range. To be conservative the ranges of both normal and log-normal formulation should be combined by using the smaller of the lower limits and higher of the upper limits.

2.4 KIT

D. G. Cacuci and M. Ionescu-Bujor [15] have presented a "rigorous methodology for computing best-estimate predictive results using experimental information in conjunction with models of time-dependent and/or stationary systems" developed at the Karlsruhe Institute of Technology (KIT) (dubbed later as KIT method). The article, where the methodology was presented, was published in 2009 and is called *Best-Estimate Model Calibration and Prediction Through Experimental Data Assimilation.*

In essence, the method uses experimental data to create better estimations of input parameter values and distributions, and similarly of output parameter uncertainties. In fact, the KIT method is very similar to the CIRCE method; it uses all the same statistical tools, but also adds some.

The KIT method provides a more rigorous mathematical background for the choices and assumptions made by CIRCE, but in the end both rely on the same

type of information. Whereas CIRCE only provides time-independent information, the KIT method offers a time-dependent system of which the time-independent option is a special case. For this reason the KIT method can also be thought of as a more general approach than the CIRCE method.

The basis of the KIT method is a procedure similar to the expectation-maximization algorithm using Bayes' theorem and a so called saddle-point method to provide the *a posteriori* distribution. The *a priori* distribution on the other hand is provided through the application of the theory of information entropy. In the special case, that prior information of the distribution consists of a mean value and a standard deviation, the theory states that a normal distribution is the most likely formulation, which is the assumption posed with CIRCE. Another assumption made by CIRCE, of linearity, is also made by the KIT method by discarding higher order terms.

All experimental data available is considered by the KIT method, whereas the CIRCE method only takes into account defined data points. Theoretically the data can be used time-dependently adjusting the input parameters, while progressing the simulations. Additionally, the KIT method provides a way for internal assessment of the consistency of the data available similarly to the residuals presented with CIRCE.

A companion paper to [15] provides a simple application of the KIT method (see [16]). The application of the method is done so as to show an analytical solution from start to finish. For this purpose a simple thermal hydraulic model has been specifically built for the application of the method. The simple model allows the use of the Adjoint Sensitivity Analysis Procedure (ASAP) to produce input parameter sensitivities, which can also be utilized with CIRCE, as discussed before. When using best-estimate thermal hydraulic codes the ASAP proves inapplicable and the sensitivities need to be calculated with the help of engineering judgment.

Due to the complexity of the KIT method, the fact that no implementation of the methodology exists for use, the problems with defining the input parameter sensitivities, as well as its similarity with CIRCE, the KIT method is not evaluated further within the context of this master's thesis. Moreover, taking into account the amount of engineering judgment required, there is inherent uncertainty with the results of the method (with the same applying to CIRCE). This means that the results are not exact and should not be treated as such, even though the formulation of the tools used are mathematically rigorous.

2.5 Application to FRIGG-2 experiments

The FRIGG loop was originally a full scale facility simulating a fuel element of the Marviken boiling heavy water reactor in steady state conditions. It consisted of a test section with 36 electrically heated 4.4 m long rods and an unheated center rod, steam separator, condenser and heat exchanger. The loop could be operated with natural or forced circulation. The maximum pressure of the loop was 100 bars and the total heating power was 8 MW. Figure 1 illustrates the configuration of the FRIGG loop and the rods in the test section. [17]

The goal of the FRIGG loop experiments was to assure that the Marviken reactor

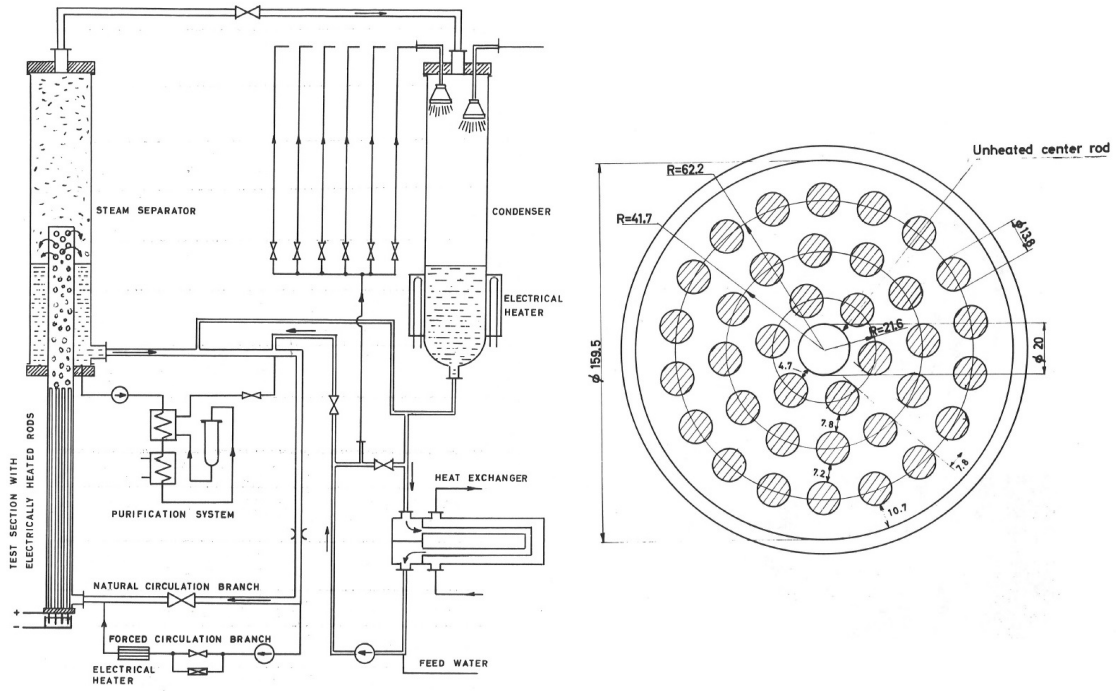

Figure 1: *FRIGG loop configuration. On the left a simplified flow diagram of the loop and on the right the configuration of the rods in the test section.* [17]

could be run safely considering fuel burnout and reactor instabilities. The project was carried out by Ab Atomenergi, ASEA and Royal Institute of Technology in Stockholm, Sweden from 1967 to 1970.

The first part of the four series of experiments in the FRIGG loop project was performed with the FRÖJÄ loop with 6-rod configuration. The other three series of experiments, which were carried out with the 36-rod FRIGG loop, were divided based on different purposes. The second series of experiments focused on hydrodynamic and heat transfer measurements with uniform heat flux distribution in the rods. These experiments were chosen for the purposes of testing the capabilities of the FFTBM and CIRCE methods with APROS due to the simplicity of the design and the availability of experimental data. However, only void fraction measurements were available for the 28 experiments included in the analyses. The boundary conditions of the experiments are presented in Table 1.

2.5.1 APROS model of the FRIGG loop

The FRIGG loop facility was modeled with APROS for the purposes of this study in a simplified form. The simulation model only includes the test section in the form of an APROS built-in *design reactor* -process component, with inlet and outlet connecting pipes. Heat structures describing the heated and center rods are also connected to the reactor component. The APROS model is shown in Figure 2.

The reactor channel is made up of 20 thermal hydraulic nodes and the rods are similarly divided into 20 axial nodes. Radially the rods are divided into 6 nodes.

Table 1: *Boundary conditions of the 28 FRIGG-loop experiments used in the analyses. Subcooling defines the temperature under saturation temperature as indicated by the experiment pressure.*

Experiment number	**Pressure (bars)**	**Subcooling (°C)**	**Heating power (kW)**	**Flow (kg/m^2s)**
313001	49.6	5	1500	1492
313003	49.6	2.6	1500	1096
313004	49.8	3.7	1500	1103
313005	49.8	3.7	1500	1110
313006	50	3.7	1500	729
313007	50	11.7	1500	1110
313008	50	4.3	3000	1471
313009	50	4.4	2980	1107
313010	50	4.6	2980	687
313011	50	4.5	4440	1443
313012	49.7	4.2	1430	1457
313013	49.7	4.6	2930	1120
313014	49.7	11	2930	1163
313015	49.7	11	2920	1163
313016	49.6	19.3	2910	1208
313017	49.6	2.4	4400	1464
313018	49.7	3.7	4390	1124
313019	49.5	8.6	4390	1177
313020	49.7	22.4	4415	1159
313024	49.7	4.2	1475	858
313027	50	4.9	2820	886
313030	50	5.1	4560	823
313034	50	4.6	1500	1012
313037	50	4.4	3000	1026
313040	50	4.4	1500	792
313043	50	3.5	3000	823
313056	49.9	9.5	3000	918
313060	49.4	10.5	1470	792

The different experiments used in the analyses are defined by different flow and temperature at the inlet, as well as pressure and heating power. These are achieved simply by varying the corresponding values in the APROS model.

2.5.2 Choice of input parameters

Common to both input uncertainty methods are the parameters that are investigated, as well as the output parameters that are used in the investigation. Since the data available from the FRIGG loop experiments is only void fractions at different elevations, in this case no further choice of output parameters needs to be made. What is required from the output parameters is that they are sensitive to the input parameters under analysis.

Contrarily, when the starting point of the analysis is the output parameters, sensitivity simulations are run to find out, which input parameters are influential. This was also the case for the current analysis. The sensitivity runs were implemented by varying each input parameter on the limits of their preliminary variation ranges

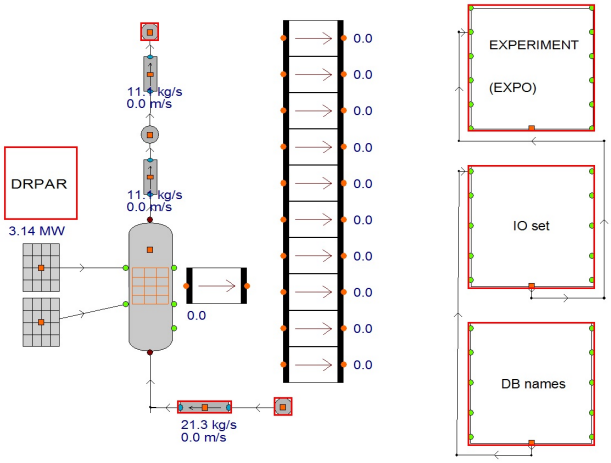

Figure 2: *FRIGG loop APROS model.*

defined by expert judgment.

Only two parameters were chosen as influential of the 25 investigated parameters related to the closure relations of the APROS code. These parameters were *interfacial friction in bubbly flow* (IF) and *heat transfer between liquid and interface* (HT). Both parameters are multipliers with the nominal value of 1. The full list of parameters is shown in Table 2.

Table 2: *List of considered input parameters.*

Parameter	**PDF type**	**Ref**	**Min**	**Max**
Minimum film boiling temperature	uniform	1	0.65	1.5
Critical heat flux	uniform	1	0.5	1.5
Interfacial friction	uniform	1	0.1	10
Interfacial friction in bubbly flow	uniform	1	0.1	10
Interfacial friction in droplet flow	uniform	1	0.1	10
Interfacial friction in annular flow	uniform	1	0.1	10
Interfacial friction in stratified flow	uniform	1	0.1	10
Wall friction coefficient / Liquid	uniform	1	0.5	2
Wall friction coefficient / Gas	uniform	1	0.5	2
Heat transfer between liquid and interface	uniform	1	0.2	5
Heat transfer between gas and interface	uniform	1	0.05	2
Heat transfer to wetted wall / Forced convection to liquid	uniform	1	0.5	1.5
Heat transfer to wetted wall / Nucleate boiling	uniform	1	0.5	1.5
Heat transfer to dry wall / Forced convection to gas	uniform	1	0.5	1.5
Heat transfer to dry wall / Pool boiling	uniform	1	0.5	1.5
Heat transfer to dry wall / Natural convection to gas	uniform	1	0.5	1.5
Quench front height	uniform	0.745	0.495	0.995
Additional heat flux near quench front (AHFNQF)	uniform	1	0.5	7.5
AHFNQF / Temperature gradient coefficient	uniform	1	0.1	1.5
Rate of entrainment	uniform	1	0.7	1.3
Rate of entrainment / Lower void limit	uniform	0.5	0.4	0.6
Rate of entrainment / Upper void limit	uniform	0.75	0.65	0.85
Max droplet diameter	uniform	1.73	1.63	1.83
Max droplet diameter above quench front	uniform	0.54	0.27	1.73
Critical Weber number for droplets	uniform	8	5	20

Whether the parameters were influential or not was defined by graphical analysis of the sensitivity run results of one experiment. The two chosen parameters caused distinctively large variations in the void fractions compared to all the other parameters. The parameter *interfacial friction* also showed large variation, but since the bubbly flow component is included in that one only the *interfacial friction in bubbly flow* was chosen as influential. The chosen parameters as well as the two largest variations after those are shown in Figure 3 for comparison.

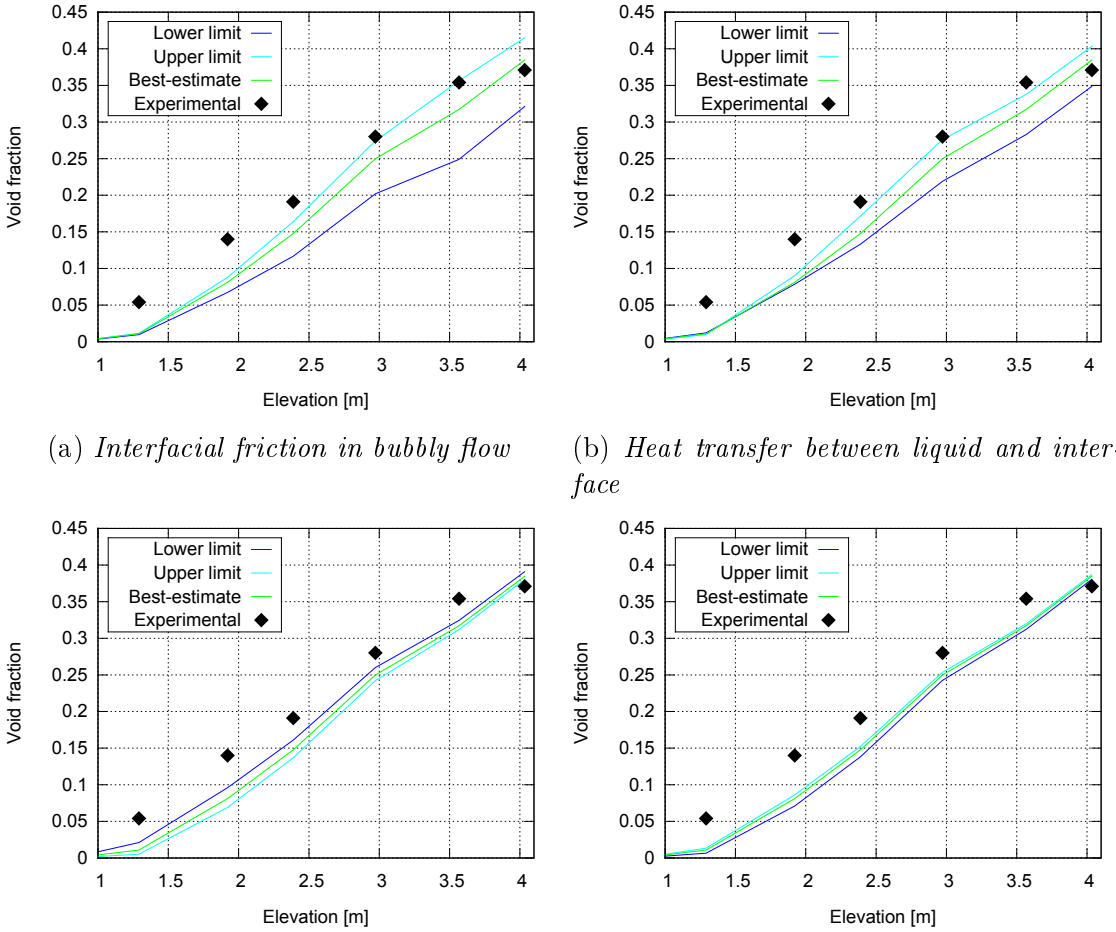

(a) *Interfacial friction in bubbly flow*

(b) *Heat transfer between liquid and interface*

(c) *Heat transfer to wetted wall / Forced convection to liquid*

(d) *Heat transfer to wetted wall / Nucleate boiling*

Figure 3: *Results of the limit runs for four different parameters, including the ones that were identified as influential (top two figures).*

2.5.3 FFTBM application and results

Due to the scarcity of data from the FRIGG-loop experiments all the data available was used in the FFTBM study. Following the steps of the application, as defined in chapter 2.2.2, the input parameters chosen in the previous section were used. Because the experiments were done in steady state, no time evolution was identified.

Instead the void fraction profiles for the different elevations of the test section for each experiment were used as if they were time evolution curves and the Fourier transform was applied to their error functions accordingly.

Void fractions under 0.2 were excluded from the data, because the correlations used by one-dimensional codes are known to underestimate void fractions at low values. Additionally, some points were discarded due to not following the general pattern of the experimental results as defined by the application of CIRCE, the results of which are shown in the next section. In practice these points were very much different from the experimental results, mostly appearing at the high end of the void fraction spectrum. The deviations could be produced, for example, by the simulation model not reproducing the experimental conditions well enough at the top end of the test section due to the simplicity of the model.

The global average amplitude was calculated by using the data from all the experiments at the same time, since with the previous definition only one output parameter could be identified for each experiment. The error function was also redefined as the closest distance from each experimental point to the calculated points. In this application this resulted in the same experimental-calculated point pairs as with the normal error function with the exception of the error values being absolute values.

To conduct the FFTBM analysis the sensitivity runs were simulated, including the reference run, for both parameters under investigation. That is, for both parameters each experiment was run 20 times varying the respective parameter with a linear spacing within its determined possible variation range. These ranges were wider than the ranges based on expert judgment would be to account for the possibility of expert judgment not being precise enough. Nevertheless, the analysis would also give reason to widen the ranges if required.

After the completion of all the runs for all the experiments the average amplitudes from each experiment for each variation of both parameters were gathered according to equation (2). These were then compiled and calculated into Global Average Amplitudes (GAA) as defined by equation (4) for each variation of both parameters and plotted. No weights were used since only one type of data was utilized. The results are shown in Figure 4.

The ranges of variation of the parameters for the application of the FFTBM method were set as [0.05, 5] and [0.05, 7] for IF and HT respectively. On the basis of the GAA curves and the threshold value, which was set to 0.3, the final ranges were identified as [0.4, 1.8] and [0.05, 2.35]. Uniform and log-normal ranges were applied to compare different formulations. The log-normal ranges were defined by finding the logarithmic mean value of the ranges and setting the standard deviation of the logarithmic distribution as half of the distance from the mean to the range limits. This way the ranges are two-sigma distance from the mean and encompass approximately 95 % of the distribution. The mean values are thus approximately 0.85 and 0.34 or on a logarithmic scale -0.164 and -1.071, while the logarithmic standard deviations are 0.376 and 0.963 respectively.

To check the created ranges 93 simulation runs were executed for each experiment with the same randomly selected values of the parameters within the new ranges.

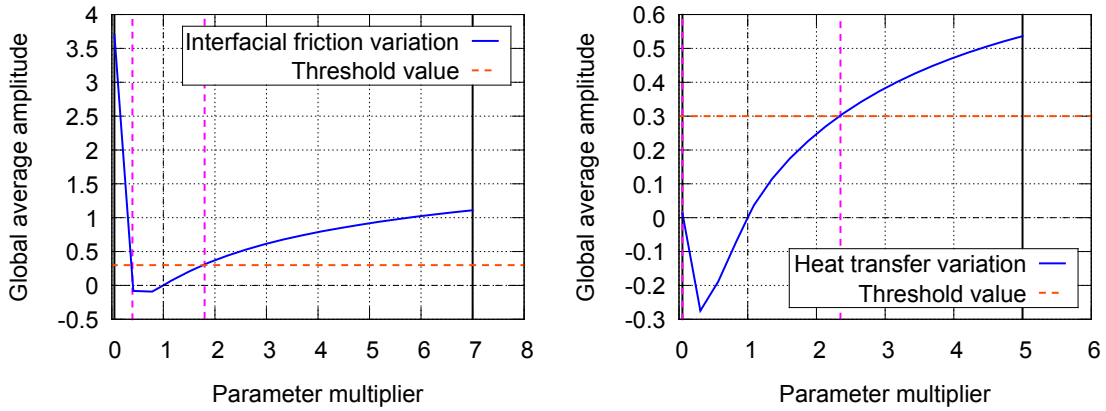

(a) *Interfacial friction in bubbly flow variation*

(b) *Heat transfer between liquid and interface variation*

Figure 4: *Results of the application of the FFTBM method to the FRIGG-2 experiments. The black lines show the original variation ranges ([0.05, 5] for IF and [0.05, 7] for HT) and the pink dashed lines the new variation ranges defined by the red dashed threshold limit line.*

According to the Wilks' formula with this amount of runs the lowest and highest values represent the 2.5 % and 97.5 % quantiles with 95 % certainty. These quantiles are supposed to envelope the experimental results for the PDFs definitions to be adequate for use. The results of the envelope calculations are presented in Figure 5.

The total amount of void fraction measurements extracted from the FRIGG-2 loop experiments was 176. Out of these 31 were below 0.2 and were discarded before the FFTBM analysis. A further 17 points were discarded on the basis of the CIRCE analysis.

Of the 128 data points left for the analysis 38 were not enveloped by the 2.5 % and 97.5 % quantiles with the uniform distribution, whereas 40 were not enveloped similarly by the log-normal distribution. Although Figure 5 shows that in general the results are good, the amount of data points on the wrong side of the bisector indicates that there is room for improving.

2.5.4 CIRCE application and results

In the application of the CIRCE method each experiment was run 5 times. 2 sensitivity runs for each parameter and a best-estimate or reference run. For both parameters the sensitivities were defined with 1 % variation in both directions.

After all the $\frac{\partial R_j}{\partial \alpha_i}$ sensitivities were derived a CIRCE input file was created and the program run. Initially all data points with a value higher than 0.2 were included in the analysis, but some of these were discarded due to their residuals (as defined by equation (14)) being higher than 2.5 and thus statistically not plausible. Several iterations were required to find a set of points that did not have any residuals over 2.5.

The results of the CIRCE application after the discarding process included very

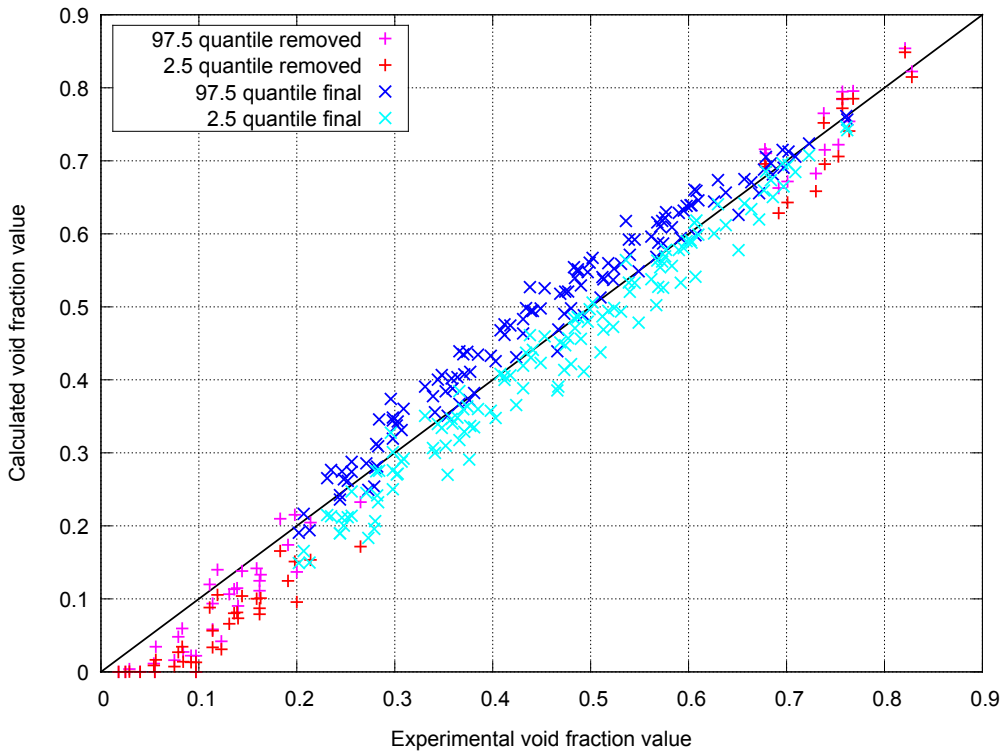

(a) *Parameter probability densities with uniform distribution.*

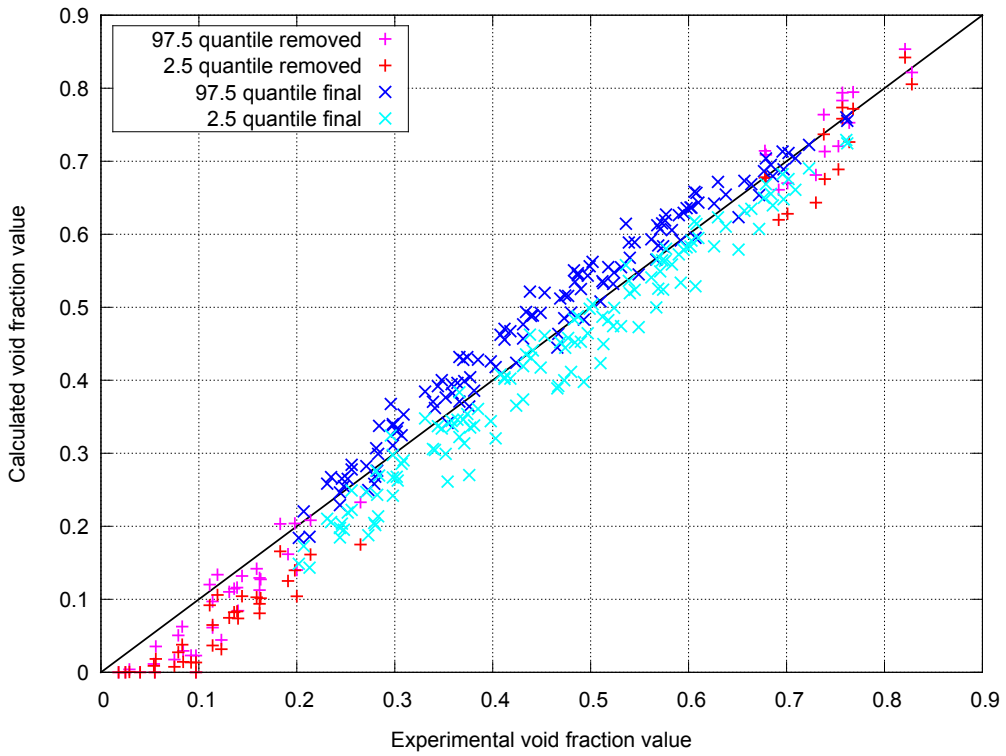

(b) *Parameter probability densities with log-normal distribution.*

Figure 5: *Results of the envelope calculations with the parameter variation ranges as defined by the FFTBM analysis showing the 2.5 % and 97.5 % quantiles as defined by the GRS method. All void fraction measurements from the FRIGG-2 loop experiments with the ones under 0.2 and selected other ones are distinguished. For both quantiles only approximately 2.5 % should be on the wrong side of the bisector, which defines perfect match between calculated and experimental results.*

high absolute biases, which inclined that CIRCE should be used iteratively. It also suggested that logarithmic formulation for the parameter PDFs should be used. This was further explored by plotting the calculated void fraction values at different parameter multiplier values. The data was the same as was used in the FFTBM application and the results are shown in Figure 6. It can be clearly seen that both parameters behave in a log-linear fashion confirming, that the use of log-normal PDFs is justified.

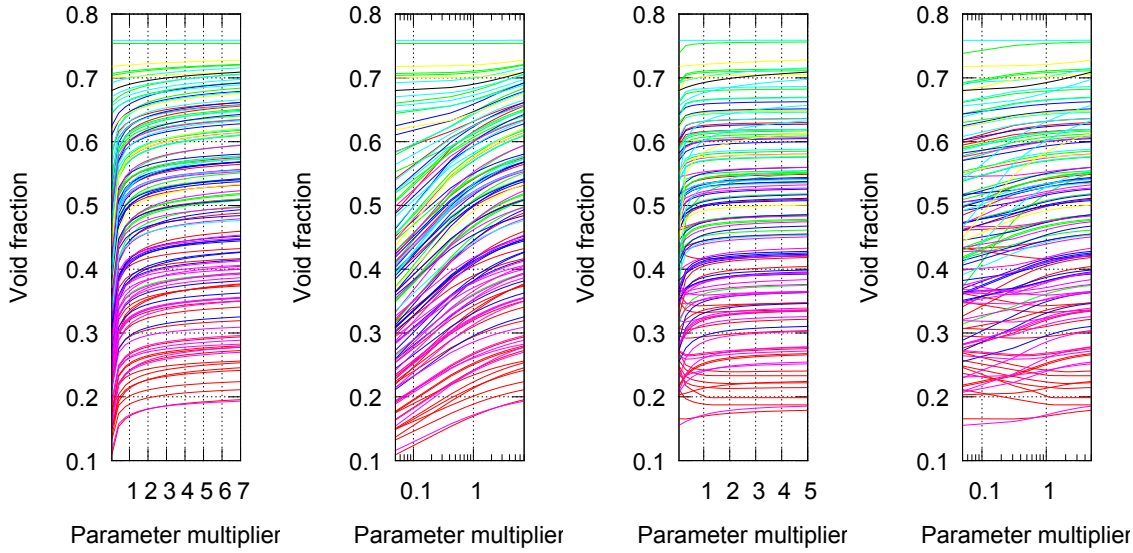

(a) *Interfacial friction normal scale* (b) *Interfacial friction logarithmic scale* (c) *Heat transfer normal scale* (d) *Heat transfer logarithmic scale*

Figure 6: *All 128 calculated void fractions at different parameter values. The data is the same as was used for the FFTBM analysis. Values can be seen to behave linearly on a logarithmic scale when comparing figure a to b and c to d.*

The CIRCE method was then iterated a few times after which it became clear that the parameter *heat transfer between liquid and interface* was not converging. However, a local equilibrium could be found. The equilibrium point was used to calculate new sensitivities by running the sensitivity simulation runs again with another 1 % variation with respect to the biased mean values. Three more iterations were required, but finally the biases converged.

The progression of the biases during the iterations can be seen in Figure 7a. Similarly, Figure 7b shows the progression of the standard deviations as printed by CIRCE. The final mean values are 0.92 and 0.28, or on a logarithmic scale -0.083 -1.273, while the logarithmic standard deviations are 0.81 and 2.52 respectively. These deviations set the ranges of the parameters with the two-sigma definition at [0.18, 4.64] and [0.002, 43.702].

Envelope calculations were again run for a final checkup of the validity of the PDFs defined with the application of CIRCE. The results are shown in Figure 8. Of the 128 points 21 are not covered by the lower and upper limits.

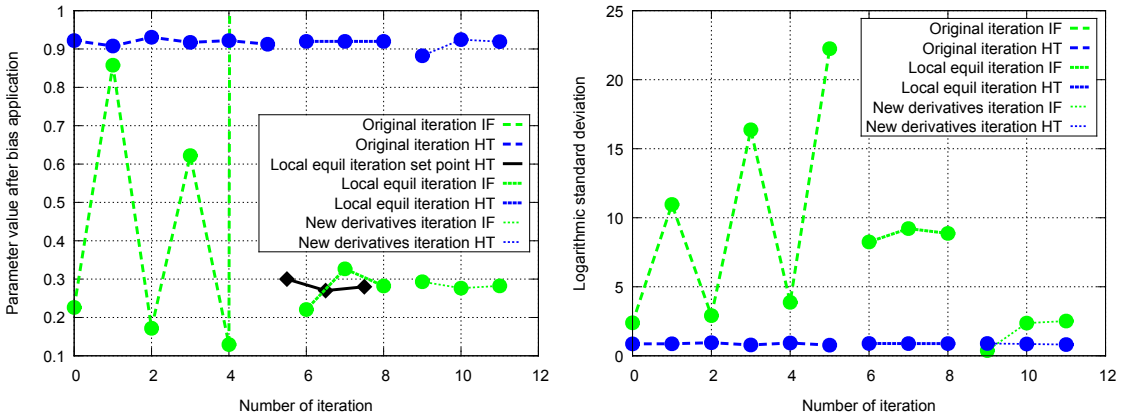

(a) *Bias development during the CIRCE iterations*

(b) *Standard deviation development during the CIRCE iterations*

Figure 7: *Results of the application of the CIRCE method to the FRIGG-2 experiments. Interfacial friction development is shown in green color and heat transfer in blue. The black color defines where the heat transfer bias was set during the iterations, when looking for local equilibrium point.*

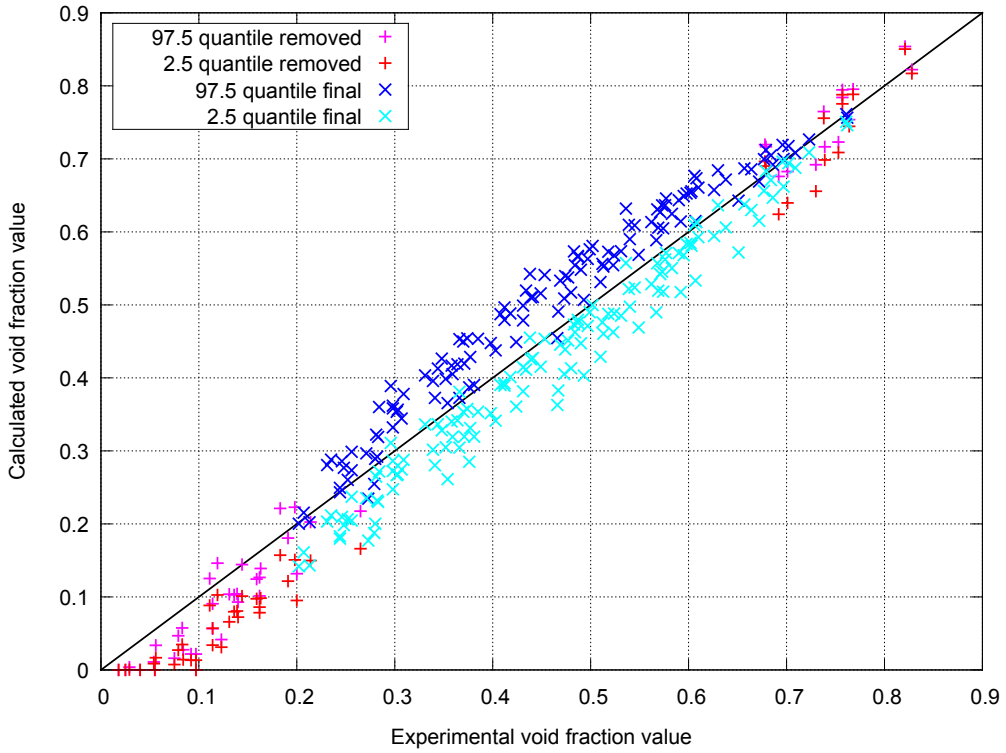

Figure 8: *Results of the envelope calculations with the parameter PDFs as defined by the CIRCE analysis showing the 2.5 % and 97.5 % quantiles as defined by the GRS method. All void fraction measurements from the FRIGG-2 loop experiments with the ones under 0.2 and selected other ones are distinguished.*

2.6 Findings

In the previous sections two methods to quantify the uncertainty of code physical models were presented in detail and a third one referenced to. The FFTBM based methodology and the CIRCE method were then applied to a simple experimental case and the results were checked with envelope calculations according to Wilks' formula for 95 %/95 % tolerance limits.

The results of the uncertainty methods are discordant to a degree. Although both methods seem to imply similar biases for the parameters, accepting values from a wider range allows for wider envelopes. This in effect nullifies the information that is gained by finding the optimal values for the biases, especially when even with the extremely wide ranges of the CIRCE application the envelope calculations still do not cover over 16 % of the experimental values.

Nevertheless, the issues faced with the results can be attributed to the particularities of the material used in the analysis. Being able to utilize only one kind of data from steady state measurements does not necessarily include enough information. Additionally unforeseen biases or uncertainties in the data could produce large shifts in the envelope calculation results. As a tool for the quantification of the uncertainties in the physical models CIRCE is very sensitive to small changes in input data due to the complex nature of its algorithms. FFTBM is not as sensitive since it essentially uses averaging over the data it is fed.

Although the results of this paradigm application of the methods are not directly usable, the findings are encouraging. Specifically, when compared, the results of the two methods provide justification for each other. As such it can be noted that according to the study performed the low quality of the data used in the analyses is generally speaking the reason for the fairly wide ranges. The lack of information can also be seen as one of the largest reasons for the envelope calculations not being good enough.

Another point to consider is that not all of the uncertainties in the APROS code were taken into account. Although only two physical model parameters were varied, others also had some influence – albeit small – and furthermore uncertainty can exist from other sources as well, as described in the beginning of section 2.1.

No obstructing problems were run into when applying the methods with APROS. A large amount of expert judgment is still required in the analyses, to a larger extent with FFTBM than with CIRCE. Some progress in this regard has already been seen with the development of the FFTBM methodology, but due to being incomplete not discussed further in this master's thesis. In regards to the CIRCE method the largest issue is with defining the derivatives, especially when the systems become more complex and are time dependent.

Both the FFTBM and CIRCE methods were found to be applicable to researching the uncertainties of the physical models of APROS. Although issues arose, there were no impediments to using the methods in the PREMIUM benchmark.

3 PREMIUM benchmark

The Post-BEMUSE REflood Models Input Uncertainty Methods benchmark is a direct succession of state-of-the-art uncertainty methods studies. It brings together the foremost experts of uncertainty studies from around the world to better the statistical sampling approach by focusing on the ways the uncertainties of input parameters can be quantified, specifically of the physical models of the codes related to reflooding calculation.

For VTT the main interest in taking part in the PREMIUM benchmark is to accumulate knowledge of the different aspects of Best-Estimate Plus Uncertainty (BEPU) studies. This includes studying the uncertainties of the physical models of the APROS thermal hydraulic system code, and the ways in which these uncertainties can be quantified and further applied to BEPU studies.

In this master's thesis the previous work conducted on the PREMIUM benchmark is briefly referred to, which includes the background of the benchmark as well as the uncertain parameter identification phase of the benchmark. Thereafter the quantification of the uncertainties is performed with the help of the FFTBM and CIRCE methods using the FEBA (Flooding Experiments with Blocked Array) reflooding experiment data. Finally, the quantified Probability Density Functions (PDFs) of the parameters are confirmed with data from the PERICLES 2D experiments.

3.1 Framework

The Best-Estimate Methods – Uncertainty and Sensitivity Evaluation (BEMUSE) pointed out that much attention should be directed on the quantification of the uncertainties of the physical models of thermal hydraulic codes, when applying the input uncertainty propagation method with statistical sampling of the parameters. The reasons behind this are that to-date no common understanding on the uncertainties of the physical models exists. In fact no common understanding on the method of quantification of the uncertainties exist either.

Historically uncertainties of the physical models have been quantified for phenomena that can be separated from other phenomena in an experimental setting. After this it is simply a matter of comparing calculated results to experimental results while varying the physical model multiplier. In the case of phenomena, which can not be experimented on with separate effect test, the situation becomes more complex.

The PREMIUM benchmark focuses on one such situation: reflooding of the nuclear reactor core after dryout following a Large Break Loss Of Coolant Accident (LBLOCA). Phenomena that take place are for example interfacial friction and heat transfer in different boiling modes, quench front propagation and associated heat transfer modifications, as well as the transitions between different boiling modes.

In the first phase of the benchmark the three uncertainty quantification methods presented in chapter 2.1 were introduced. Other ways of quantifying the uncertainties were also identified, which could be grouped under expert judgment, comprising

for example of "trial-and-error", definition of biases and experience from code use.

Initially the method chosen by VTT for quantifying the uncertainties of the input parameters was expert judgment. This choice was based on the lack of experience on the use of the methods, which begged for the exertion of expert judgment. Also, biases existed in the APROS code, which hindered the use of both CIRCE and FFTBM methods.

During the course of the project some bugs were found and corrected in the APROS code, which altered the best-estimate results and removed some of the biases. The corrections changed the results to the extent that both FFTBM and CIRCE methods could be applied to some degree. In addition, the knowledge gained while performing the work presented previously in this master's thesis helped in the application of the methods.

3.2 Identification

The first part in quantifying the uncertainties of the physical models within the PREMIUM benchmark was to identify, which models are influential in the reflooding scenario under investigation. The German FEBA experiments conducted in the 1980's were chosen for these purposes. A recap of the identification phase of the PREMIUM benchmark is described below, while it is explained more thoroughly in [18].

3.2.1 FEBA model

The experimental arrangement consisted of a 4.114 m long reactor channel with 5-by-5 3.9 m long electrically heated rods with a cosine axial power profile. The test series focused on blocked setups imitating core meltdown, but the experiments used in the PREMIUM benchmark were without blockage. The boundary conditions of the six experiments used in the benchmark are shown in Table 3.

Table 3: *Boundary conditions of the FEBA experiments used in the PREMIUM benchmark [19].*

Test No.	**Inlet velocity (cm/s)**	**System pressure (bar)**	**Feed water temperature (°C)**		**Bundle power (kW)**	
			0-30 s	**End**	**0 s**	**Transient**
214	5.8	4.1	45	37	200	120% ANS
216	3.8	4.1	48	37	200	120% ANS
218	5.8	2.1	42	37	200	120% ANS
220	3.8	6.2	49	37	200	120% ANS
222	5.8	6.2	43	36	200	120% ANS
223	3.8	2.2	44	36	200	120% ANS

A model of the experimental facility was built with APROS, which can be seen in Figure 9. In the model the rods were defined by 10 radial and 78 axial heat structure nodes connected with heat transfer in both radial and axial directions. The

reactor channel was described as a pipe element divided into 78 thermal-hydraulic nodes with additional nodes in the ends. The reactor channel was surrounded by a housing simulated with 2 x 80 heat structure nodes. Seven grid spacers inside the channel were modeled by reducing the channel area, introducing a higher pressure loss coefficient and a smaller hydraulic diameter.

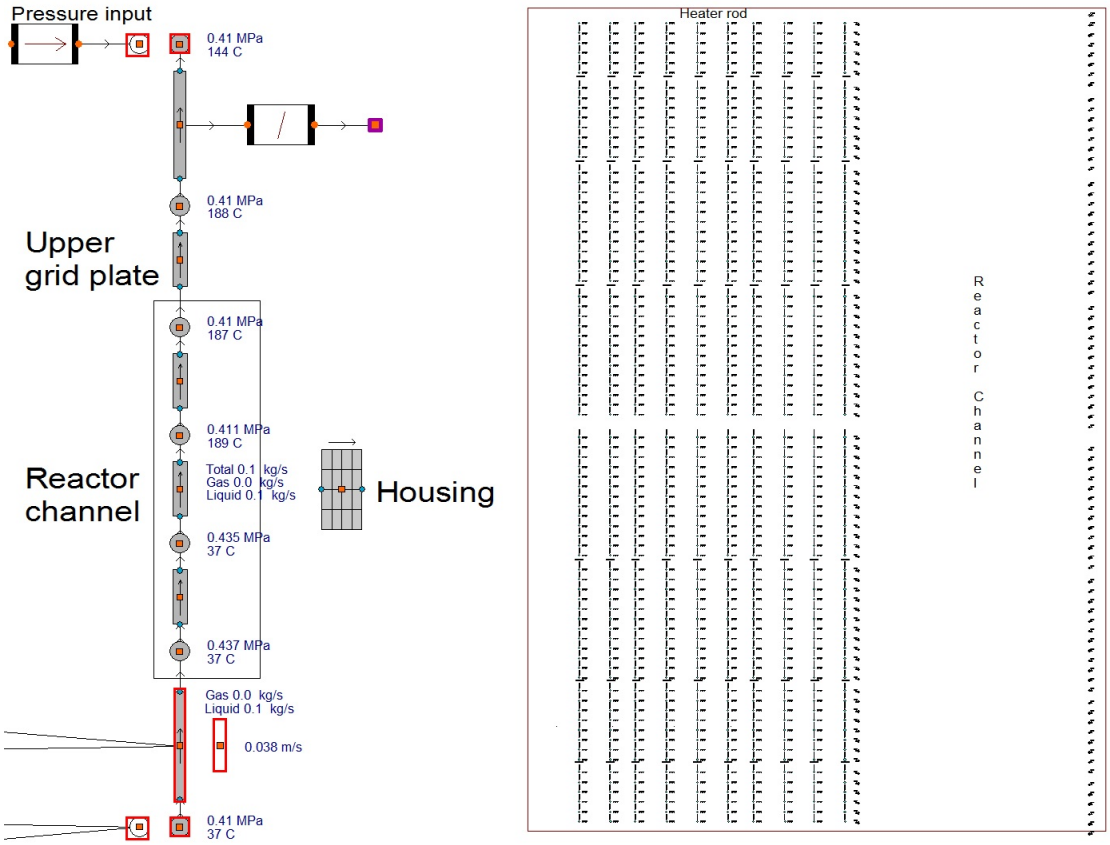

Figure 9: *APROS model of the Flooding Experiments with Blocked Array experimental setup. On the left is shown the reactor channel setup and on the right the structure of the rods and the heat transfer modules to the reactor channel.*

The experiment starts with the reactor channel full of steam and the rods at high temperature simulating the heat up due to decay heat in a reactor after loss of coolant. Thereafter water input to the channel is started from the bottom. Gradually the water level rises causing rapid steam production as the water rewets the rods and the channel housing. In such conditions practically all thermal-hydraulic phenomena modeled with APROS take place.

In the APROS model the water being injected into the reactor channel needs to fill a small thermal-hydraulic node before touching the hot rods. During this time the rods keep on heating rapidly without the cooling effect of droplets passing through the channel. On the other hand, it seems that the experimental data starts at the point, where the water touches the rods.

The time the water takes to fill the node was not taken into account in the

following analyses with the APROS model due to it being realized too late in the analysis. This results in a bias in the calculated values due to the excess heat in the system. The situation is presented qualitatively for three different elevations in the case of cladding temperatures in Figure 10.

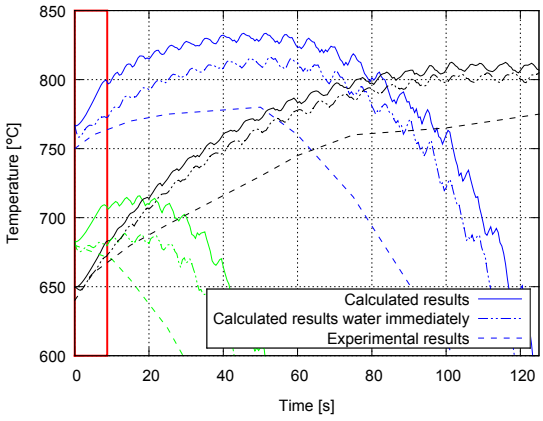

Figure 10: *Qualitative differences between experimental and calculated values of cladding temperatures at different elevations, with both the setup used in the analyses and with one where the water does touch the rods immediately. The red box highlights the beginning of the transient before the water touches the rods in the used setup. The green lines are for a low elevation, the blue ones for a center elevation and the black ones for a high elevation.*

Although the difference does not seem to be large, it is prominent in the beginning of the transient and for lower elevations. The product is higher temperatures and later rewetting times.

3.2.2 PREMIUM Phase II results

To identify, which phenomena and, thus, physical models are important, sensitivity runs of the experiment number 216 were run while varying each input parameter on the upper and lower limits of their predefined PDFs. The distributions at this point were based on expert judgment and were all set as uniform within certain ranges. Additionally, all physical parameters that could have had influence on the results were varied similarly. All the parameters that were considered are shown in Table 4.

The parameters that fit set criteria were identified as influential and were moved to the next phase of the benchmark for quantification of their uncertainties. None of the physical parameters were found to be influential. The selected parameters and their PDFs, or in this case ranges, are shown in bold in Table 4.

3.2.3 After Phase II

During the preparatory work for Phase III of the PREMIUM benchmark, or quantification of the uncertainties, the list of parameters chosen for quantification was modified from the one reported after Phase II. Four parameters were dropped, namely:

Table 4: *List of input parameters considered in the PREMIUM benchmark Phase II. VTT reported results of the identified influential input parameters are shown in bold. Ref, or reference, is the best-estimate value and min and max define the range limits.*

Parameter	PDF type	Ref	Min	Max	Mean	Stdev
Channel free flow area	normal	0.00389	0.00359	0.0042	0.0039	0.00015
Channel hydraulic diameter	normal	0.01344	0.01244	0.0144	0.0134	0.0005
Housing thickness	normal	7.03822	6.83822	7.2382	7.0382	0.1
Inlet water velocity	normal	0.038	0.03686	0.0391	0.038	0.00057
System pressure	normal	0.41	0.4	0.42	0.41	0.005
Inlet water temperature	uniform	1	0.9	1.1		
Rod power	normal	1	0.95	1.05	1	0.025
Channel form loss coefficient	uniform	0	0	1		
Grid spacer form loss	uniform	1.5	0.5	2		
Grid spacer area	normal	0.00311	0.00292	0.0033	0.0031	9.7E-05
Grid spacer hydraulic diameter	normal	0.00645	0.00613	0.0068	0.0065	0.00016
Rate of entrainment	**uniform**	**1**	**0.7**	**1.3**		
Rate of entrainment / Lower void limit	uniform	0.5	0.4	0.6		
Rate of entrainment / Upper void limit	uniform	0.75	0.65	0.85		
Wall friction coefficient / Liquid	**uniform**	**1**	**0.5**	**2**		
Wall friction coefficient / Gas	uniform	1	0.5	2		
Minimum film boiling temperature	**uniform**	**1**	**0.65**	**1.5**		
Heat transfer to wetted wall / Forced convection to liquid	uniform	1	0.5	1.5		
Heat transfer to wetted wall / Nucleate boiling	uniform	1	0.5	1.5		
Heat transfer to dry wall / Pool boiling	uniform	1	0.5	1.5		
Heat transfer to dry wall / Forced convection to gas	**uniform**	**1**	**0.5**	**1.5**		
Heat transfer to dry wall / Natural convection to gas	uniform	1	0.5	1.5		
Additional heat flux near quench front	**uniform**	**1**	**0.5**	**7.5**		
AHFNQF / Temperature gradient coefficient	uniform	1	0.1	1.5		
Max droplet diameter	uniform	1.73	1.63	1.83		
Max droplet diameter above quench front	**uniform**	**0.54**	**0.27**	**1.73**		
Critical Weber number for droplets	uniform	8	5	20		
Heat transfer between liquid and interface	uniform	1	0.2	5		
Heat transfer between gas and interface	**uniform**	**1**	**0.05**	**2**		
Critical heat flux	**uniform**	**1**	**0.5**	**1.5**		
Interfacial friction	**uniform**	**1**	**0.1**	**10**		
Quench front height	**uniform**	**0.745**	**0.495**	**0.995**		
Fuel rod filler heat capacity density	uniform	1	0.95	1.05		
Fuel rod filler thermal conductivity	uniform	1	0.8	1.2		
Fuel rod heater / cladding heat capacity density	uniform	1	0.95	1.05		
Fuel rod heater / cladding thermal conductivity	uniform	1	0.93	1.07		
Housing heat capacity density	uniform	1	0.95	1.2		
Housing thermal conductivity	uniform	1	0.95	1.05		
Rod initial temperatures	uniform	1	0.995	1.005		
Housing initial temperatures	uniform	1	1.00	1.04		

rate of entrainment, *max droplet diameter above quench front*, *critical heat flux* and *quench front height*.

This was due to a bug that was found in the calculation of entrainment, which caused some physical models to be calculated wrong in reflooding conditions. The differences can be seen in Figure 11. Thus new sensitivity runs were performed and with the same criteria for parameter influence as were used in Phase II the parameters *rate of entrainment*, *critical heat flux* and *quench front height* were dropped from the list of influential parameters.

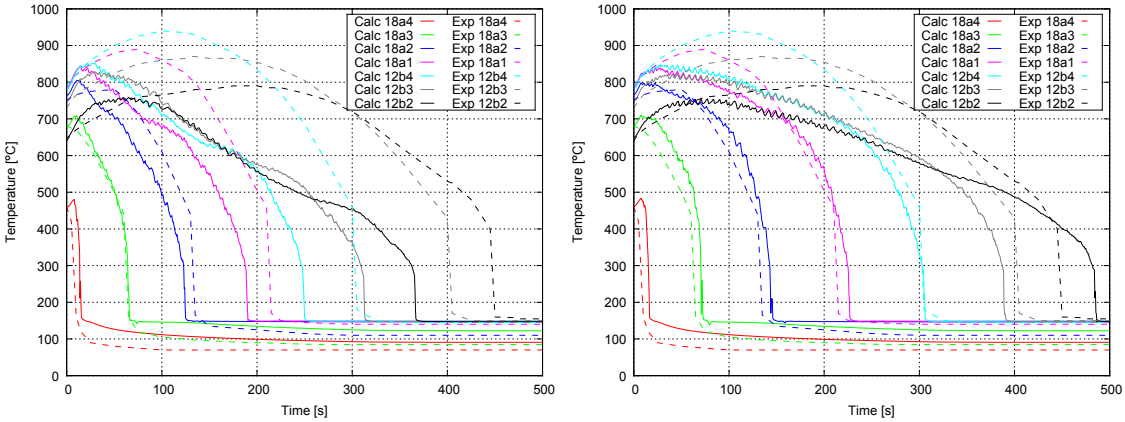

Figure 11: *FEBA experiment number 216 cladding temperatures before (left) and after (right) modifications to the APROS code.*

A decision was made to drop the parameter *max droplet diameter above quench front* also, since there were dependencies with other parameters, mainly with *interfacial friction*. In the case of interfacial friction it was also noted that only the interfacial friction related to droplets, which occurs above the quench front, was influential and thus it was determined to only vary that component. The decision was partly based on other benchmark participants having reached similar conclusions. The final list of parameters chosen for quantification is shown in Table 5.

Table 5: *Final list of identified influential input parameters to be quantified in Phase III of the PREMIUM benchmark. Ref, or reference, is the best-estimate value and min and max define the range limits.*

Parameter	**PDF type**	**Ref**	**Min**	**Max**
Wall friction coefficient / Liquid	uniform	1	0.5	2
Minimum film boiling temperature	uniform	1	0.65	1.5
Heat transfer to dry wall / Forced convection to gas	uniform	1	0.5	1.5
Additional heat flux near quench front	uniform	1	0.5	7.5
Heat transfer between gas and interface	uniform	1	0.05	2
Interfacial friction droplet	uniform	1	0.1	10

3.3 Quantification

For the quantification of the uncertainty of the parameters both CIRCE and FFTBM were utilized. Additionally several thousands of simulations were run while randomly varying all parameters with the idea of finding out, which possible combinations of the varied parameters could produce results that were consistent with experimental values.

None of the methods provided reasonable results on their own; all had their deficiencies. FFTBM was not able to capture some biases that were known to exist in the code, CIRCE failed in providing meaningful standard deviations and the random simulations were found to be excessively costly considering computer time to see through and showed signs of not converging. Thus, an effort was made to produce a quantification of the parameter uncertainties with the help of all available and achievable information in a cost effective way.

The logic of the final quantification was roughly the following. CIRCE was used to find the biases (or mean values) of the parameters. With the help of the knowledge gained from the random simulations, biases that were known to exist in the code and running some checkup runs, a best-estimate of the parameter biases was tuned. Then, the FFTBM method was employed, taking into account the biases, and this way ranges for the PDFs were found.

3.3.1 Random variation application and results

A total of 4053 simulations of the experiment number 216 were run while randomly varying the parameters in each run with Latin Hypercube Sampling (LHS). In LHS the PDF is divided into as many equally probably blocks as there are runs and then a block and the value inside it is chosen randomly. The consistency of the simulation results were checked with a Root Mean Square (RMS) distance of the experimental points from the closest calculated points (taking into account both time and magnitude variation).

Threshold values for the RMS for different outputs were defined by performing a 93 run BEPU analysis of the experiment number 216 while varying only the parameters that were deemed uninfluential in the identification phase. Specifically, the RMS distances of the lower and upper bounds of the uninfluential parameters BEPU analysis to the best-estimate run results were used to specify the thresholds. For cladding temperatures slightly tighter threshold was adopted than the RMS suggested. The BEPU analysis results of the four parameters used in checking the consistency are shown in Figure 12.

Of the list of parameters that were not deemed influential some were dropped, namely entrainment related parameters as well as the ones that were dropped due to dependencies to other parameters. The list of parameters that were varied, with their PDFs, is shown in Table 6.

The 4053 runs were split into three approximately equal size sets with different ranges of variation for the parameters. The first ranges were the ones defined with expert judgment and presented in section 3.2.3. The values of the parameters in the

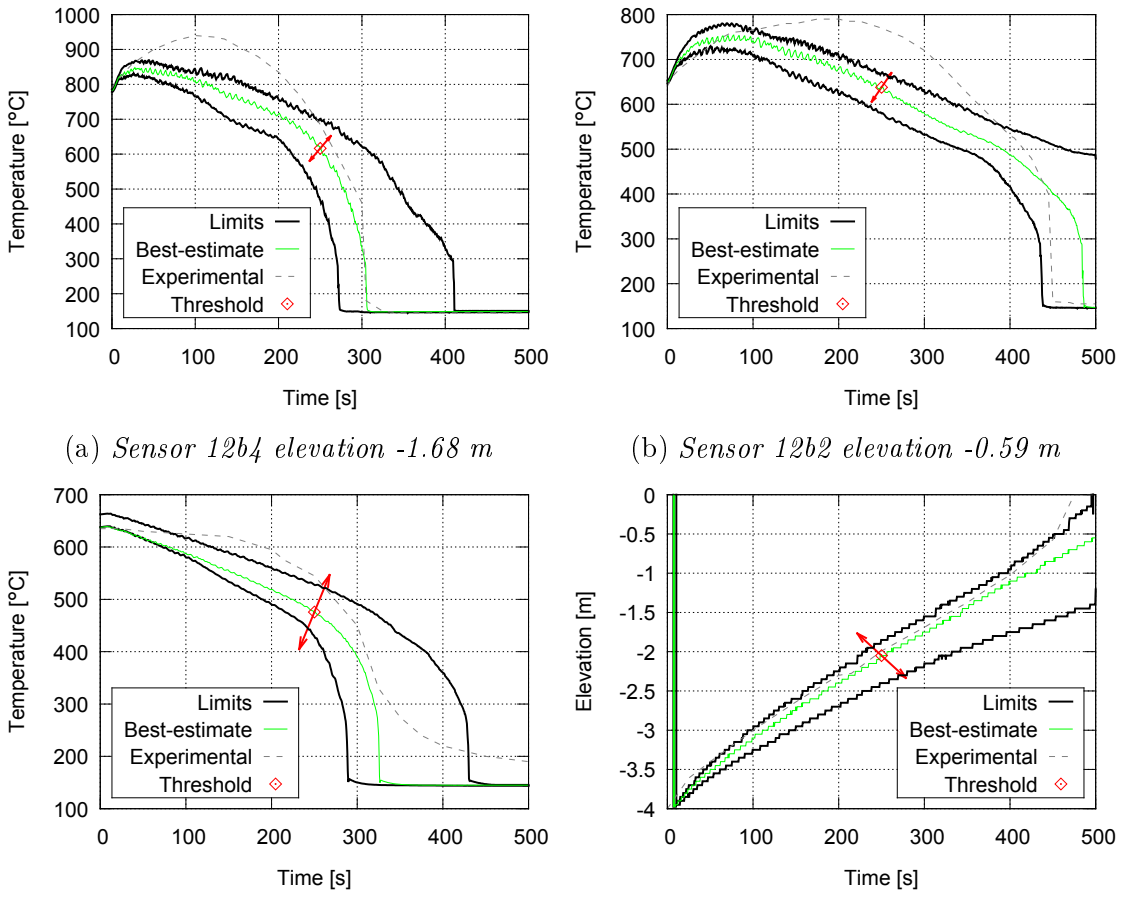

(a) *Sensor 12b4 elevation -1.68 m*

(b) *Sensor 12b2 elevation -0.59 m*

(c) *Housing at elevation -1.725 m*

(d) *Quench front propagation*

Figure 12: *FEBA experiment number 216 uninfluential parameter BEPU analysis results for cladding temperatures (a, b), housing temperature (c) and quench front propagation (d). The thresholds are shown to represent their magnitude and do not represent anything in terms of position or direction.*

runs consistent with experimental results were collected and the means and standard deviations for each parameter were calculated.

The new ranges were set at $[\text{mean} - 2\sigma, \text{mean} + 2\sigma]$ on a normal scale, although logarithmic scale was also calculated. If the new ranges did not exceed the previous ones, the ranges were not changed to maximize the lack of knowledge. The ranges were defined similarly after the second set of simulations was run. The results of the random variation runs are presented in Table 7.

As can be seen from the results the ranges keep on growing, which suggests that no convergence could be found. Still, some ranges are never met, more precisely the lower limits of *minimum film boiling temperature* and *additional heat flux near quench front*, as well as the higher limit of *heat transfer to dry wall/forced convection to gas*. Additionally, strong correlations could be found between for example *additional heat flux near quench front* and *interfacial friction droplet*. More information would be gathered by further simulations, but due to the cost of the simulations

Table 6: *The input parameters and their PDFs used for assigning threshold values for RMS in the random variation simulation runs.*

Parameter	PDF type	Ref	Min	Max	Mean	Stdev
Critical heat flux	uniform	1	0.5	1.5		
Quench front height	uniform	0.745	0.495	0.995		
Interfacial friction bubbly	uniform	1	0.1	10		
Interfacial friction annular	uniform	1	0.1	10		
Wall friction coefficient / Gas	uniform	1	0.5	2		
Heat transfer to wetted wall / Forced convection to liquid	uniform	1	0.5	1.5		
Heat transfer to wetted wall / Nucleate boiling	uniform	1	0.5	1.5		
Heat transfer to dry wall / Pool boiling	uniform	1	0.5	1.5		
Heat transfer to dry wall / Natural convection to gas	uniform	1	0.5	1.5		
AHFNQF / Temperature gradient coefficient	uniform	1	0.1	1.5		
Heat transfer between liquid and interface	uniform	1	0.2	5		
Channel free flow area	normal	0.00389	0.00359	0.0042	0.0039	0.00015
Channel hydraulic diameter	normal	0.01344	0.01244	0.0144	0.0134	0.0005
Housing thickness	normal	7.03822	6.83822	7.2382	7.0382	0.1
Inlet water velocity	normal	0.038	0.03686	0.0391	0.038	0.00057
System pressure	normal	0.41	0.4	0.42	0.41	0.005
Inlet water temperature	uniform	1	0.9	1.1		
Rod power	normal	1	0.95	1.05	1	0.025
Channel form loss coefficient	uniform	0	0	1		
Grid spacer form loss	uniform	1.5	0.5	2		
Grid spacer area	normal	0.00311	0.00292	0.0033	0.0031	9.7E-05
Grid spacer hydraulic diameter	normal	0.00645	0.00613	0.0068	0.0065	0.00016
Fuel rod filler heat capacity density	uniform	1	0.95	1.05		
Fuel rod filler thermal conductivity	uniform	1	0.8	1.2		
Fuel rod heater / cladding heat capacity density	uniform	1	0.95	1.05		
Fuel rod heater / cladding thermal conductivity	uniform	1	0.93	1.07		
Housing heat capacity density	uniform	1	0.95	1.2		
Housing thermal conductivity	uniform	1	0.95	1.05		
Rod initial temperatures	uniform	1	0.995	1.005		
Housing initial temperatures	uniform	1	1	1.04		

and the apparent non-convergence of the ranges, this particular study was stopped after the third iteration.

3.3.2 FFTBM application and results

Two main differences to the FFTBM method as presented by University of Pisa were introduced during its application. First, the error function defining the difference between calculated and experimental results was produced by calculating the shortest distance from each experimental point to the calculated points (taking into account both time and magnitude variation). Second, the Global Average Amplitude (GAA) was calculated considering all the different experiments at once, instead

Table 7: *Random variation run results for the six parameters under investigation for the three iterations.*

	Wall friction coefficient / Liquid	Minimum film boiling temperature	Heat transfer to dry wall / Forced convection to gas	Additional heat flux near quench front	Interfacial friction droplet	Heat transfer between gas and interface
Ranges set for first round						
Min	0.5	0.65	0.5	0.5	0.1	0.05
Max	2	1.5	1.5	7.5	10	2
First round results, Total runs: 1300 **Consistent:** 47						
Linear						
Min	0.451	0.668	0.313	1.610	0.340	-0.060
Max	2.169	1.599	1.267	8.645	5.664	1.470
Logarithmic						
Min	0.588	0.719	0.437	2.079	1.061	0.198
Max	2.580	1.710	1.320	10.933	6.924	1.879
Ranges set for second round						
Min	0.45	0.65	0.3	0.5	0.1	0.05
Max	2.2	1.6	1.5	8.65	10	2
Second round results, Total runs: 1313 **Consistent:** 52						
Linear						
Min	0.407	0.652	0.0979	1.878	-0.220	-0.113
Max	2.298	1.803	1.370	9.319	7.066	1.688
Logarithmic						
Min	0.560	0.710	0.280	2.300	1.082	0.190
Max	2.833	1.996	1.601	11.864	8.372	2.300
Ranges set for third round						
Min	0.4	0.65	0.1	0.5	0.1	0.05
Max	2.3	1.8	1.5	9.3	10	2
Third round results, Total runs: 1440 **Consistent:** 55						
Linear						
Min	0.560	0.746	0.079	1.318	0.025	-0.127
Max	2.591	1.982	1.290	10.404	8.402	1.953
Logarithmic						
Min	0.668	0.816	0.248	1.787	1.176	0.194
Max	3.251	2.157	1.552	15.424	11.413	2.915

of output parameters for just one experiment.

The first change was adopted, because the simple error function overemphasizes the timing of rewetting and thus does not fit well in studying reflooding cladding temperatures. The difference is depicted in Figure 13. The second approach resulted from its ability to take into account several experiments at once. It is neither seen as having adverse effects since, in practice, the data is similar in magnitude and time scale in all experiments.

To derive the data required to calculate GAA values all six experiments were simulated for each parameter with seven different values. The seven values were linearly spaced between the identified ranges and all the other parameters were held constant at their best-estimate values. Additionally, a best-estimate run was performed.

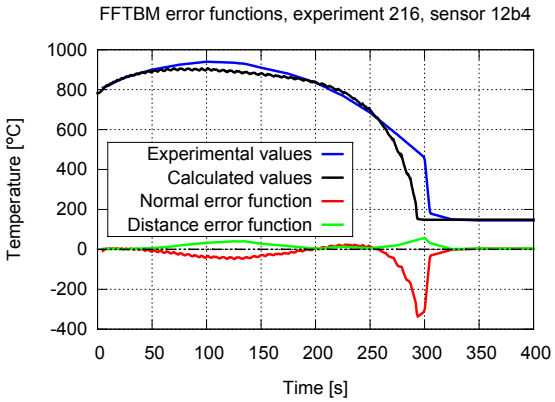

Figure 13: *The difference between simple error function and distance error function.*

Then the average amplitudes for selected output parameters were calculated. The parameters were cladding temperatures 18a1, 12b4 and 12b2 at elevations -2.225 m, -1.68 m and -0.59 m respectively, housing temperature at elevation -1.725 m and quench front propagation. Finally, all average amplitudes were combined to calculate the GAA for all parameters at the different values. The results can be seen in Figure 14.

It can be seen from the results, that for three parameters (Figures 14b, 14d and

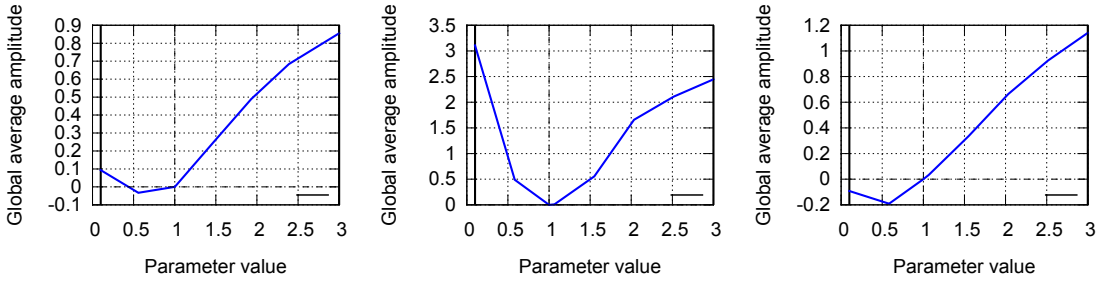

(a) *Wall friction coefficient / Liquid*

(b) *Minimum film boiling temperature*

(c) *Heat transfer to dry wall / Forced convection to gas*

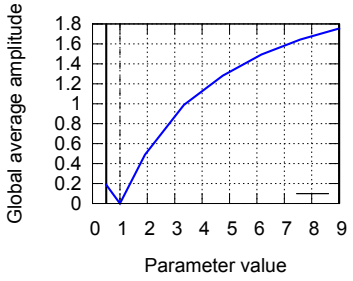

(d) *Additional heat flux near quench front*

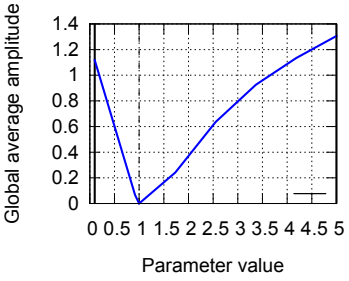

(e) *Interfacial friction droplet*

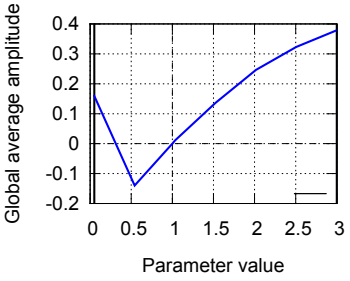

(f) *Heat transfer between gas and interface*

Figure 14: *Original FFTBM analysis results for the different input parameters.*

14e) the best fit to experimental results is found at the nominal parameter value of 1. For the other three (Figures 14a, 14c and 14f) the FFTBM analysis suggests large biases.

The biases of the parameters could have large effects on the best-estimate results, and thus on the GAA values for all parameters. For this reason the analysis was repeated with new best-estimate values of the previously identified parameters. The results for the second iteration of the FFTBM are presented in Figure 15. The best-estimate values for the two iterations of the FFTBM method are shown in Table 8.

Table 8: *Best-estimate (or reference) values of the input parameters after the first and second iteration of the FFTBM method. N/A means not applicable, because it could not be defined.*

Iter#	Wall friction coefficient / Liquid	Minimum film boiling temperature	Heat transfer to dry wall / Forced convection to gas	Additional heat flux near quench front	Interfacial friction droplet	Heat transfer between gas and interface
1st	0.7	1	0.5	1	1	0.5
2nd	1.5	1.5	1	2	1	N/A

It is evident from the results that the optimal parameter values are jumping from side to side. This indicates that the FFTBM method does not work adequately when the reference, or best-estimate, simulation results are not sound compared to the

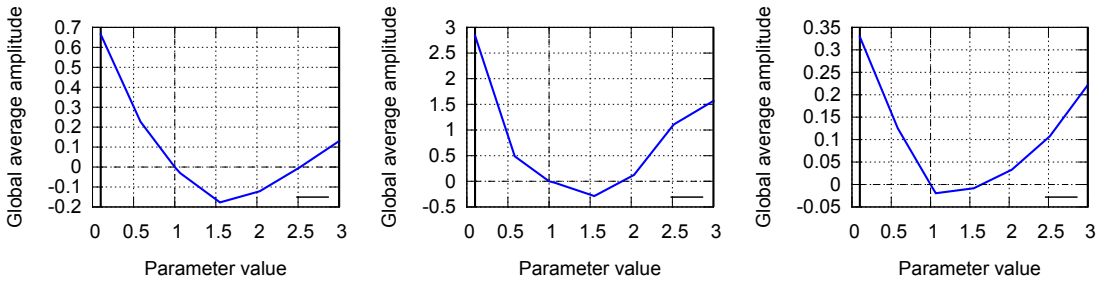

(a) *Wall friction coefficient / Liquid* (b) *Minimum film boiling temperature* (c) *Heat transfer to dry wall / Forced convection to gas*

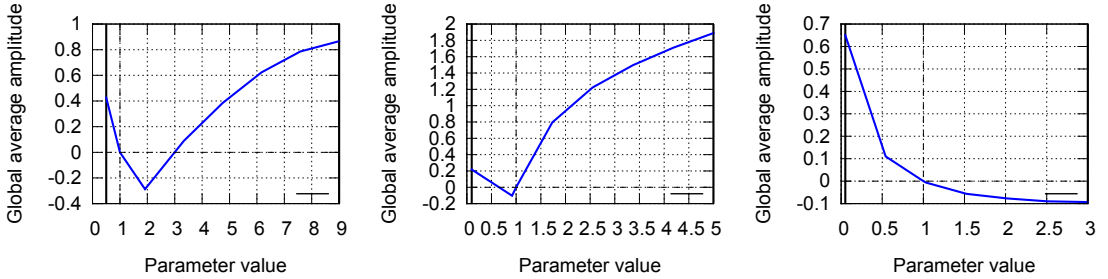

(d) *Additional heat flux near quench front* (e) *Interfacial friction droplet* (f) *Heat transfer between gas and interface*

Figure 15: *Second FFTBM analysis results for the different input parameters.*

experimental results. If there would only be one parameter that was biased, it could still be revealed with the FFTBM. In the current case with several biases, further iterations of the FFTBM method would only be run to try to find the correct values for them. This would be extremely expensive in computing time due to the amount of sensitivity simulations in each iteration being $6 * 6 * 7 = 252$, while other means – for example CIRCE and trial and error – can be used more efficiently.

3.3.3 CIRCE application and results

To provide the derivatives required by CIRCE each of the six FEBA experiments used in the PREMIUM benchmark were run 13 times. Two times for negative and positive increments for each parameter and a best-estimate run. First the output points and the increments needed to be defined, though, to be able to extract usable, consistent data.

The output points were defined by choosing some of the experimental data points and observing how the calculated results behaved in their vicinity. A total of 12 output points were chosen for each experiment. For all experiments the points were cladding temperatures at three different times and three different elevations, housing temperature at -1.725 m at a particular time, and rewetting time instant at two elevations. The cladding temperatures from elevations -2.225 m, -1.680 m and -0.590 m were used for all experiments, whereas the time instants for the cladding and housing temperatures as well as rewetting elevations varied from experiment to experiment based on the availability of data and the timescales of the events in the experiments.

To define the increments that would produce best data a trial and error approach was used. The experiment number 214 was used in the definition. The difficulty of defining the derivatives was that the calculation results oscillated in time, with each parameter producing different changes in the oscillations with different increments. Figure 16 portrays examples of the impact of different increments at a particular output point, namely the point of cladding temperature at axial level -0.590 m. It is defined as the maximum value in the time range from 55.75 s to 62.25 s, while the experimental point is at 60 s.

The definition of a time range around the experimental point was required due to the oscillations. In general the idea was to capture the trend over time of the results and because of that the range most often had to cover at least one full oscillation. In some cases the minimum value in the range, instead of maximum, was also used, because it illustrated the differences better, or because it produced better results when reviewing all the different input parameters. Due to technical reasons the same time range was used for all six input parameters, but this did not seem to hamper the results extensively.

Figure 16 showcases some of the issues with defining the derivatives. The Figures 16a and 16b were produced with very small increments, whereas Figures 16c and 16d with large ones. With the small increments, the outputs behave erratically. The results of the different simulation runs overlap and the trends for both negative and positive increments seem to be higher than the best-estimate run. Moreover, the

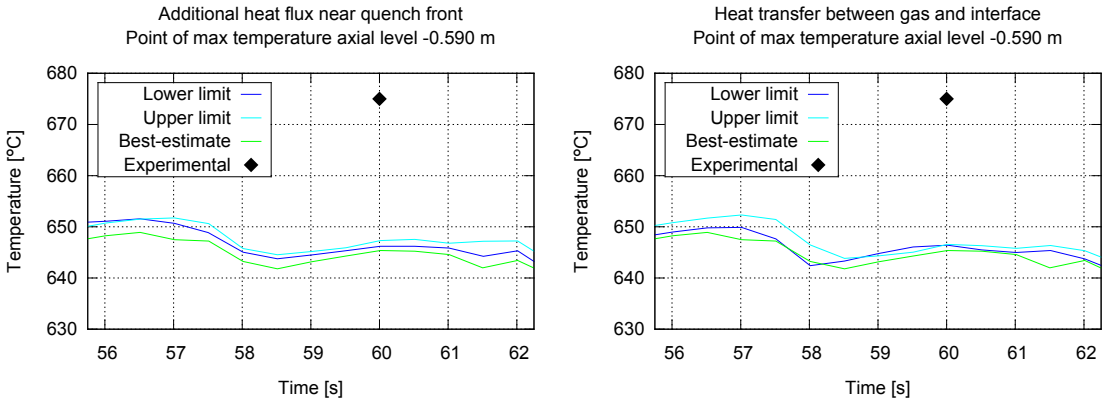

(a) *Lower: 0.999. Upper: 1.001*

(b) *Lower: 0.999. Upper: 1.001*

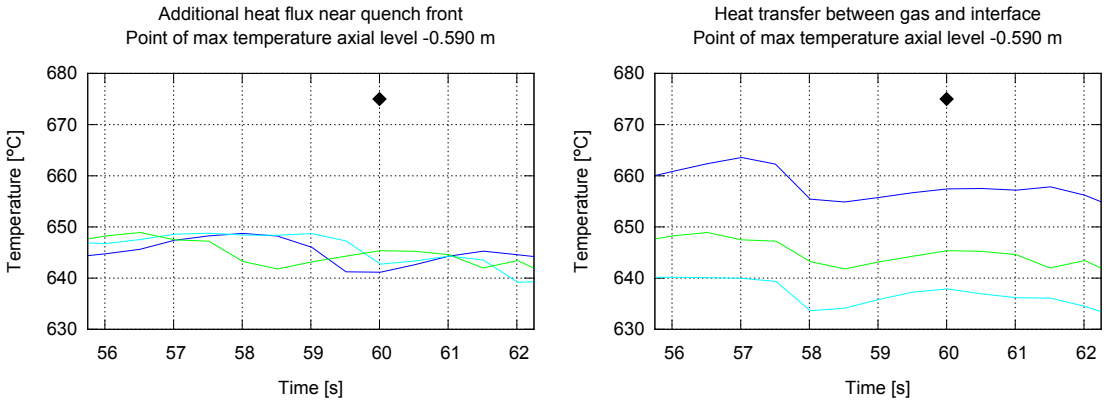

(c) *Lower: 0.8. Upper: 1.5*

(d) *Lower: 0.8. Upper: 1.2*

Figure 16: *Examples of defining derivatives with different increments. FEBA experiment number 214 cladding temperature at axial level -0.590 m in the time range from 55.75 s to 62.25 s is shown.*

derivatives produced with the small increments are extremely large compared to the larger increments.

Figure 16c proves that unlike the small increment results suggest, the particular parameter does not seem to have any effect on the magnitude of the output, but only shifts the oscillations. The Figure 16d on the other hand demonstrates, that negative and positive increments in fact lead the results in different directions, and offers a clear view of the derivative in this particular case.

The derivatives themselves were quantified as the difference between the output values extracted for the negative and positive increments divided by the difference between the increments. Figure 17 shows a few examples of the derivatives defined by the difference to the best-estimate run for both positive and negative increments, which should be of approximately the same size for a particular output point, since the final derivative will essentially be the average of the two.

As can be seen in Figure 17 the derivatives defined by the small increments were in this case mostly opposite to each other and around 1000 times larger than the

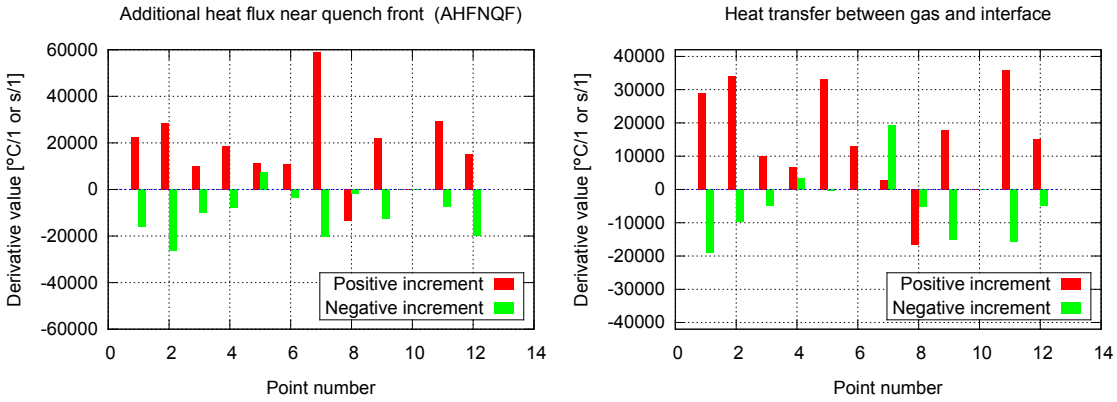

(a) *Lower: 0.999. Upper: 1.001*

(b) *Lower: 0.999. Upper: 1.001*

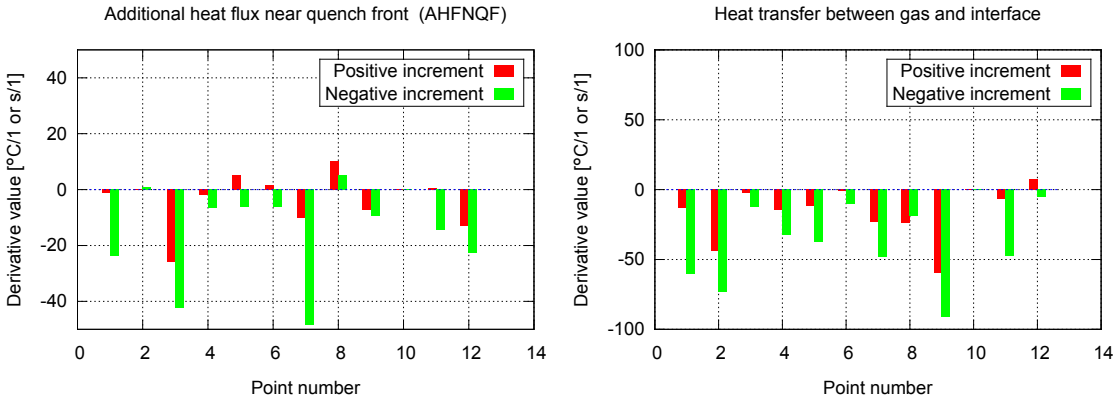

(c) *Lower: 0.8. Upper: 1.5*

(d) *Lower: 0.8. Upper: 1.2*

Figure 17: *Examples of defining derivatives with different increments. Positive and negative increment results for all 12 points in FEBA experiment number 214 are shown.*

ones defined by larger increments. The larger ones did not produce perfect results either, but were still reasonable considering that the time ranges also had to be the same for all input parameters. The final variations of the parameters for the definition of the derivatives are shown in Table 9.

Table 9: *Final input parameter variation (increment) values for the definition of the derivatives for the first application.*

	Wall friction coefficient / Liquid	Minimum film boiling temperature	Heat transfer to dry wall / Forced convection to gas	Additional heat flux near quench front	Interfacial friction droplet	Heat transfer between gas and interface
Lower	0.9	0.8	0.9	0.8	0.9	0.8
BE	1	1	1	1	1	1
Upper	1.1	1.2	1.1	1.5	1.1	1.2

With the derivatives having been gathered, the data was input to CIRCE for calculation. After the initial results an iteration run was performed with the original derivatives, but with the biases produced by CIRCE. Additionally, new derivatives were defined using the biases produced with the original run, and CIRCE was again run with two further iterations. Log-linear formulation for the parameters was used.

Up to 9 output points were dropped during the iterations because their residuals were higher than 2.5. These points were mainly ones, where the input parameters' derivatives were near zero. For example cladding temperatures early on in the simulation.

The results can be seen in Figure 18 with the original CIRCE results as iteration number 0 and the two different first iterations at number 1. The one, where new derivatives was used continues on to iteration number 2 and 3.

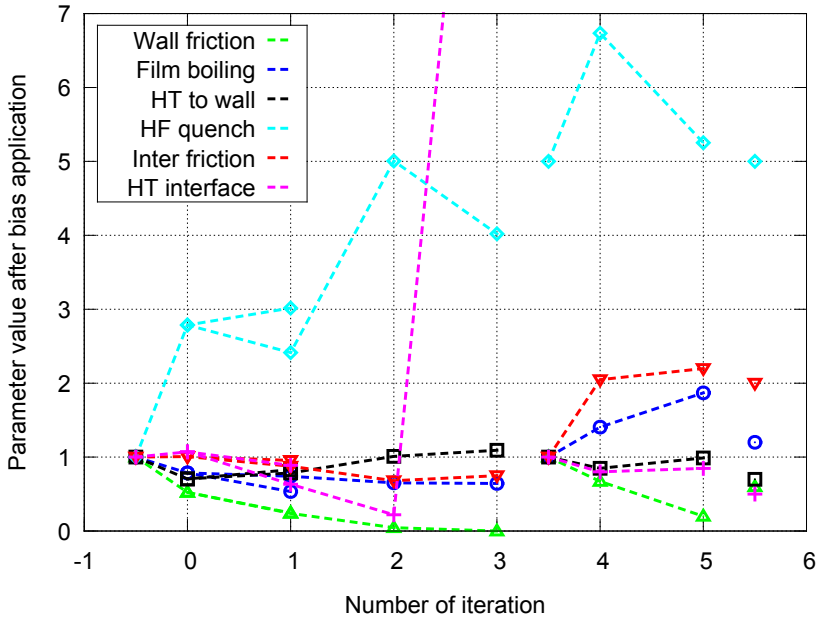

Figure 18: *Input parameters' mean value evolution during the CIRCE application.*

At iteration number 3 (second iteration with new derivatives) the parameters *minimum film boiling temperature* and *heat transfer between gas and interface* show such high divergence, that a new approach was required. For iteration number 4 all other parameters were set at 1, whereas the parameter *additional heat flux near quench front* was set to 5 due to a known bias, and new derivatives were calculated. The CIRCE analysis performed seemed to provide sensible results of the biases and a new iteration was executed.

Iteration 5 results still did not seem to converge, especially in the case of parameters *wall friction coefficient* and *minimum film boiling temperature*. Additionally the standard deviations that were produced were also nonsensical as portrayed in Figure 19, with several showing a value close to 0. For this reason a decision was made to define the final biases (iteration number 5.5 in Figure 18) with sensitivity runs of the experiment number 216 and the final PDF ranges being quantified using

the FFTBM method as described in the next section.

The sensitivity runs with the experiment number 216 were performed with the goal of optimizing the calculated results in respect to the experimental ones. Here, knowledge gained from the random variation application was used in addition to all other knowledge of the code, and from the APROS model of the facility. Only a visual analysis of the match was performed.

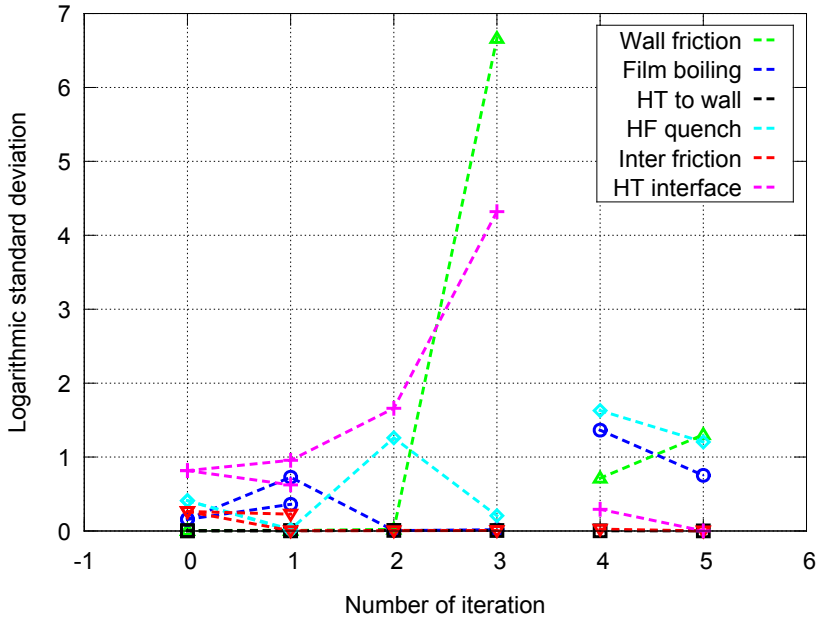

Figure 19: *Input parameters' logarithmic standard deviation value evolution during CIRCE application.*

3.3.4 Final application and results

The final ranges of the input parameter variation were decided to be defined with the application of the FFTBM method. For this purpose the reference run for FFTBM was simulated with the mean, or reference values defined with the help of CIRCE and expert judgment as presented in the previous section. The results of the FFTBM analysis are presented in Figure 20. The reference values are listed in Table 10 with the final formulation of the input parameter PDFs.

It can be seen in Figure 20, that the lowest GAA values are still not achieved at the reference parameter value for all input parameters. In the case of most parameters the results are very close to this, though, and for the rest the results are also acceptable. Further fine tuning of the reference values could be performed, but was not deemed necessary considering the additional computer time required, the schedule of the PREMIUM benchmark and the minimal improvement of the results that would have been possible with the additional analysis.

Envelope calculations of experiment number 216 were used to define the GAA threshold value, trying with both all uniform and normal or log-normal PDFs of the

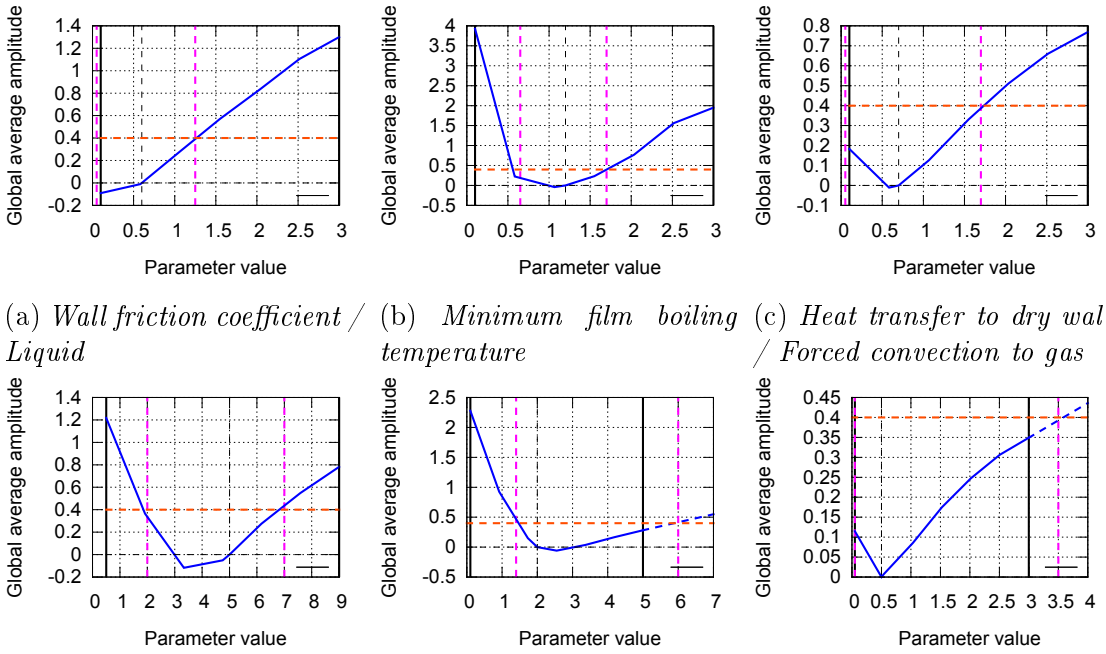

(a) *Wall friction coefficient / Liquid*

(b) *Minimum film boiling temperature*

(c) *Heat transfer to dry wall / Forced convection to gas*

(d) *Additional heat flux near quench front*

(e) *Interfacial friction droplet*

(f) *Heat transfer between gas and interface*

Figure 20: *Final FFTBM analysis results for the different input parameters. The blue lines represent the GAA values with the different parameter values, although in figures (e) and (f) the dashed blue line represents a linear extrapolation. The black vertical lines define the original variation range whereas the dashed pink lines are the new ranges achieved with the acceptability threshold shown with the red dashed line. The dashed black lines emphasize the zero-line and the reference values of the parameters.*

parameters. The same acceptability threshold for GAA was applied for all the input parameters when defining the ranges of parameter variation from the results of the FFTBM method application. The envelope calculation results are shown in Figure 21 for the same output parameters as were used in the FFTBM application.

The process of choosing the threshold limit was started with a supposed high conservatism; the threshold value of 0.5 gave wide ranges of the input parameters. Uniform distribution was tried for the same reason. As can be seen in Figure 21 the first results of the envelope calculations gave very wide upper and lower bounds. This was considered as excessive and the threshold value for the AAG was lowered twice, before choosing the final set of normal and log-normal distributions for the input parameter PDFs.

In the case of the final PDF formulation the lower threshold limit of 0.3 proved to be unduly constrictive as the lower bounds of the temperatures did not encompass all experimental values (see cladding temperature 18a1 and quench front propagation in Figure 21 top and bottom row, second subfigures from the right).

The final forms of the distributions were defined by using the FFTBM sensitivity runs to find out whether the relationships between the input parameters and output

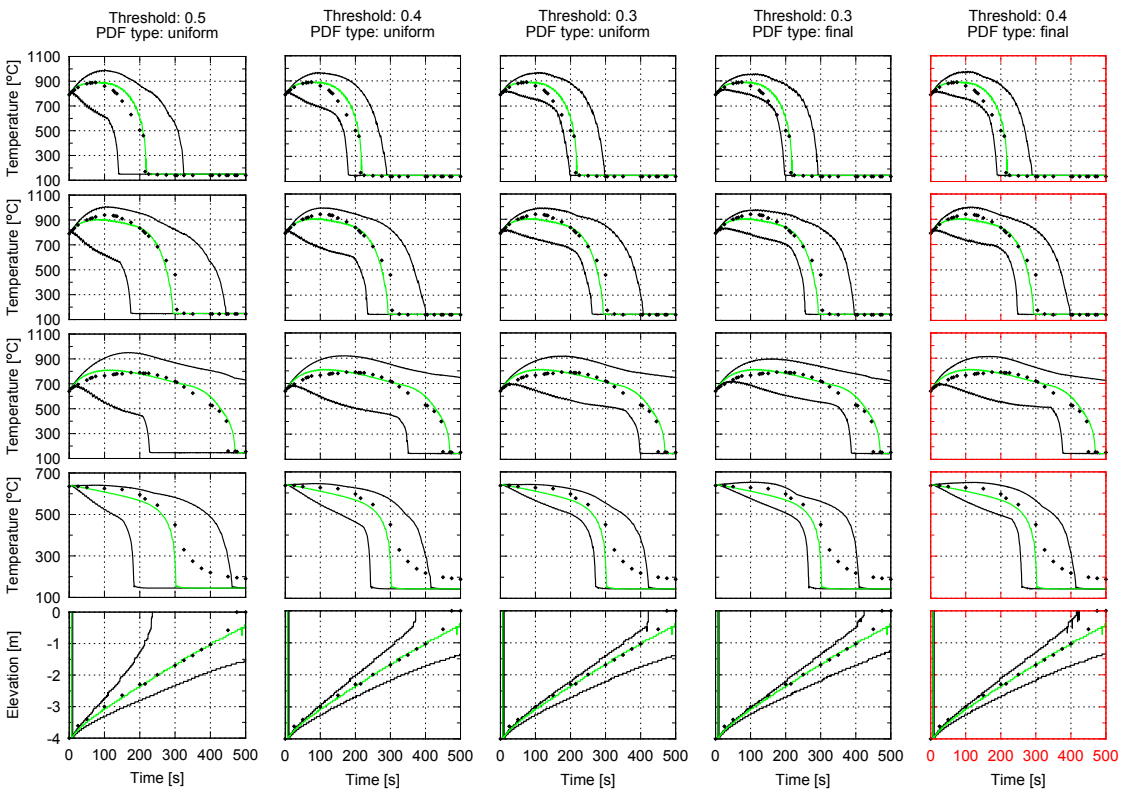

Figure 21: *Envelope calculation results reading from the top row to the bottom for cladding temperatures 18a1, 12b4 and 12b2 at elevations -2.225 m, -1.68 m and -0.59 m respectively, housing temperature at elevation -1.725 m and quench front propagation. The succession of different threshold values and PDF formulation develops from the left to right. The black lines in the figures are the lower and upper bounds, the black dots are experimental results and the green line is the reference calculation result. The final choice of PDF formulation and threshold value is shown on the right with red border.*

points used in the application of CIRCE were linear or log-linear. The ranges of the distributions achieved with FFTBM were used as 2-sigma ranges as applicable according to the form of the distributions. The results of the sensitivity runs with the chosen relationships can be seen in Figure 22.

The x-axes in the sub-figures of Figure 22 are set according to the ranges extracted from Figure 20. Thus, linearity is required in the area shown, while outside of the ranges the output point values may behave non-linearly in the chosen linear or logarithmic scale. It can be noted that not all of the output points in the case of all parameters seem to behave linearly in the chosen scale. Total accordance is not required, though, and a formulation that generally speaking shows the best fit to linearity is to be chosen.

Table 10 presents the final results of the PDFs with the acceptability threshold of the GAA set at 0.4 and the PDF types set according to the relations extracted from the FFTBM sensitivity runs with the help of the CIRCE output points.

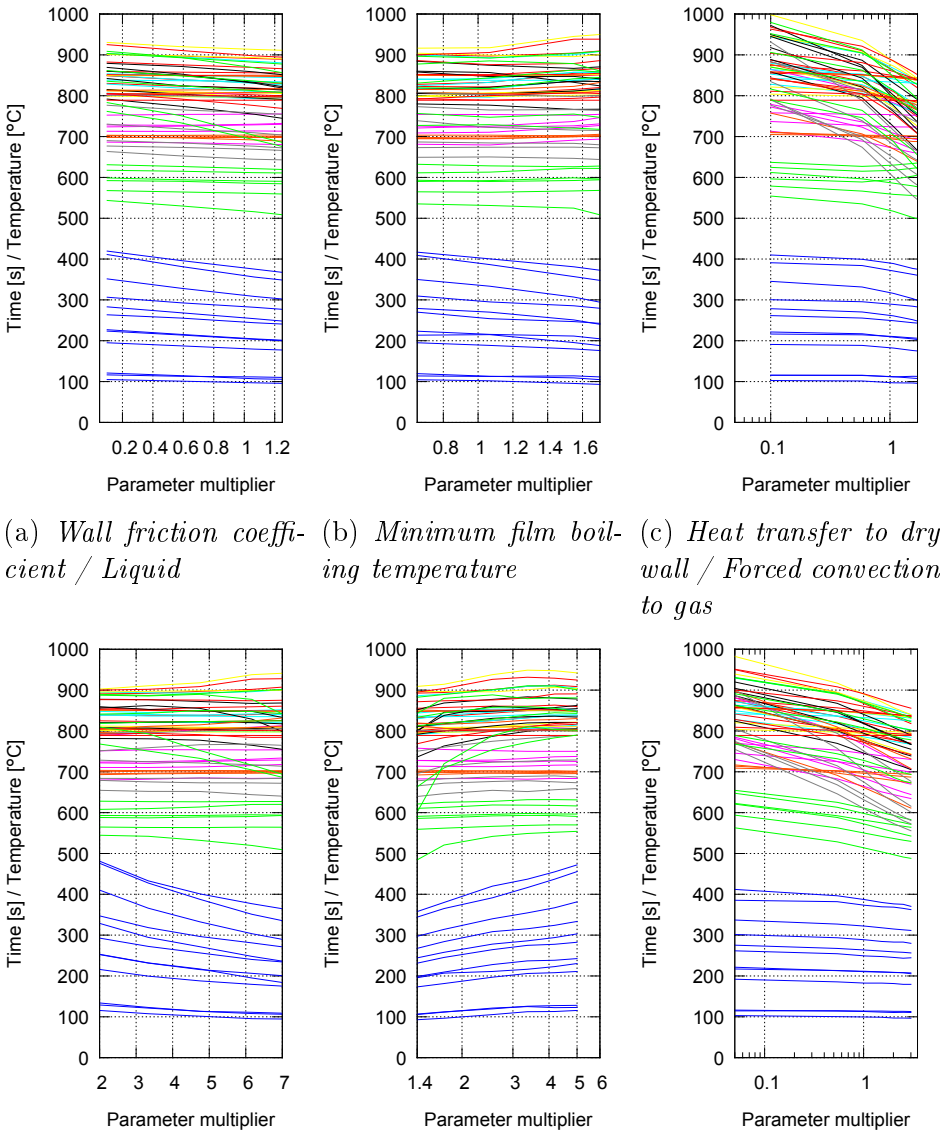

(a) *Wall friction coefficient / Liquid*

(b) *Minimum film boiling temperature*

(c) *Heat transfer to dry wall / Forced convection to gas*

(d) *Additional heat flux near quench front*

(e) *Interfacial friction droplet*

(f) *Heat transfer between gas and interface*

Figure 22: *Sensitivity run results of the input parameters for the CIRCE points with either linear or log-linear formulation accordingly. (a), (b) and (d) are shown on a linear scale and (c), (e) and (f) on a logarithmic scale. The blue lines in the bottom of each figure are times and all the others temperatures.*

The most important remark to make from Table 10 is that in the case of two parameters, namely *additional heat flux near quench front* and *interfacial friction droplet*, the original best-estimate value of 1 is not included in the variation ranges. Even if the original best-estimate values were included the normal formulation of the distributions would assure that they would be highly unlikely to be achieved. As a result these are seen as the two largest biases in the calculations.

To check that the PDF formulations were correctly drafted, envelope runs were

Table 10: *Final input parameter probability distribution function definitions. The original expert judgment PDFs are also shown for reference. For the new final formulation the mean values are the same as the reference values on a linear scale, while they are reported according to the PDF type. Similarly the standard deviations are reported in their respective scales, whereas the minimum and maximum values are on a linear scale for all parameters.*

	Wall friction coefficient / Liquid	Minimum film boiling temperature	Heat transfer to dry wall / Forced convection to gas	Additional heat flux near quench front	Interfacial friction droplet	Heat transfer between gas and interface
Original formulation						
PDF	uniform	uniform	uniform	uniform	uniform	uniform
Ref	1	1	1	1	1	1
Min	0.5	0.65	0.5	0.5	0.1	0.05
Max	2	1.5	1.5	7.5	10	2
New final formulation						
PDF	normal	normal	log-normal	normal	log-normal	log-normal
Ref	0.6	1.2	0.7	5	2	0.5
Mean	0.6	1.2	-0.36	5	0.69	-0.69
Stdev	0.275	0.25	0.44	1.25	0.55	0.97
Min	0.05	0.65	0.05	2	1.4	0.05
Max	1.25	1.7	1.7	7	6	3.5

also performed for the remaining five experiments. The results are shown in Figure 23 with the help of the output points chosen in the CIRCE application.

Only one output point was removed from the total of 72 points during the last phase of the CIRCE application based on its residual being over 2.5. This was due to very small derivatives of all the input parameters in respect to the particular point. It can also be seen in Figure 23, as both the 2.5 % and 97.5 % quantiles for this point are practically on top of each other around the 800 degree Celsius mark.

Eight of the points shown in Figure 23 are on the wrong side of the bisection; specifically all of eight points are of the 2.5 % quantile and are thus above the bisector. Seven of the points are cladding temperatures selected from very early stages of the transient, where the variation from the reference calculations are smaller. The eighth point is a rewetting time from a low elevation.

All the eight points can be explained by the reference calculation not being close enough to the experimental values. In this case it is mainly due to the discrepancy between the APROS model and the experimental setup, with the time of the water touching the rods being different as explained in section 3.2.1.

All in all, the output points behave as they should; they are approximately evenly distributed above and below the bisector. Additionally, taking into account the discrepancies in early behavior of the transients in the APROS model, the points confirm that the formulation of the input parameter PDFs is pertinent in the case of the FEBA experiment, allowing the move to the next phase of the PREMIUM benchmark, the confirmation.

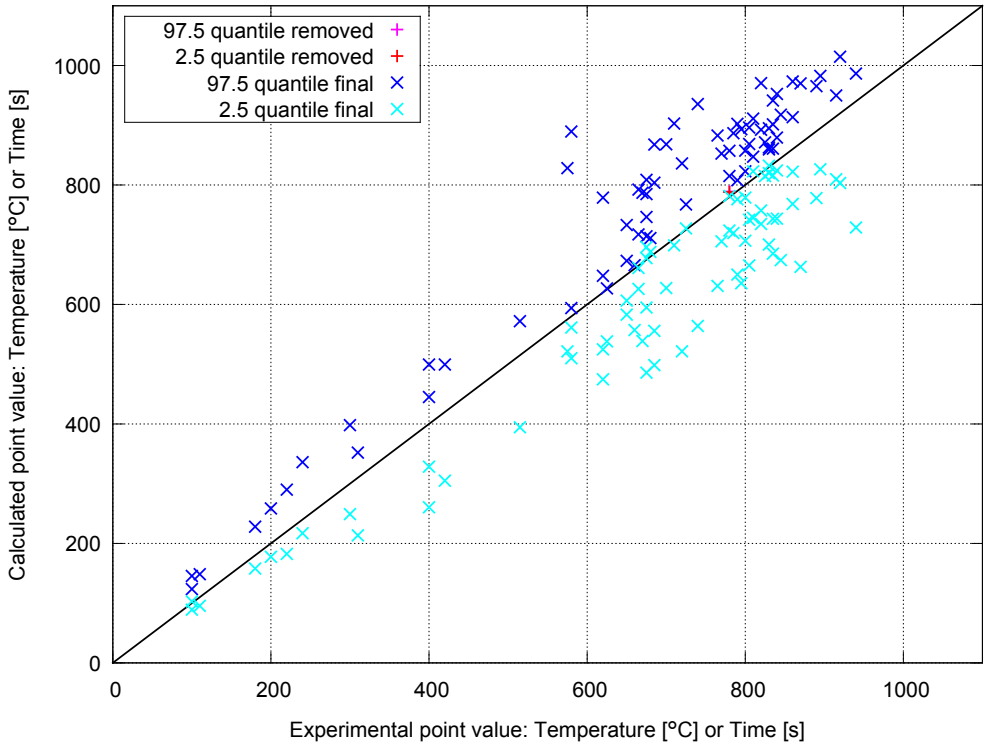

Figure 23: *Results of the envelope calculations with the parameter PDFs as defined by the final analysis showing the 2.5 % and 97.5 % quantiles as defined by the GRS method.*

3.4 Confirmation

The fourth phase of the PREMIUM benchmark consists of building a simulation model of the PERICLES 2D facility and running BEPU analysis of several reflooding experiments performed at the facility during the 1980's. This master's thesis includes a description of the facility and the APROS model, the validation of the model against some experimental data that was made available to benchmark participants and a preliminary BEPU analysis result of one of the experiments that will be submitted to the benchmark organizers. At the moment of writing the Phase IV is still ongoing and thus no comparison with experimental results is performed here.

3.4.1 PERICLES 2D facility

The PERICLES 2D facility [20] was built with the purpose of investigating thermal hydraulic phenomena in a reflooding situation in radial direction. Most experiments before PERICLES had used tubes or single bundles, which mainly exhibit axial phenomena. In a real nuclear reactor core, on the other hand, radial phenomena occurs also due to radial power distribution. The PERICLES experiments were conducted to help determine whether radial phenomena exist and need to be addressed by thermal hydraulic system codes, and how they could be addressed if required. A diagram of the facility is shown in Figure 24.

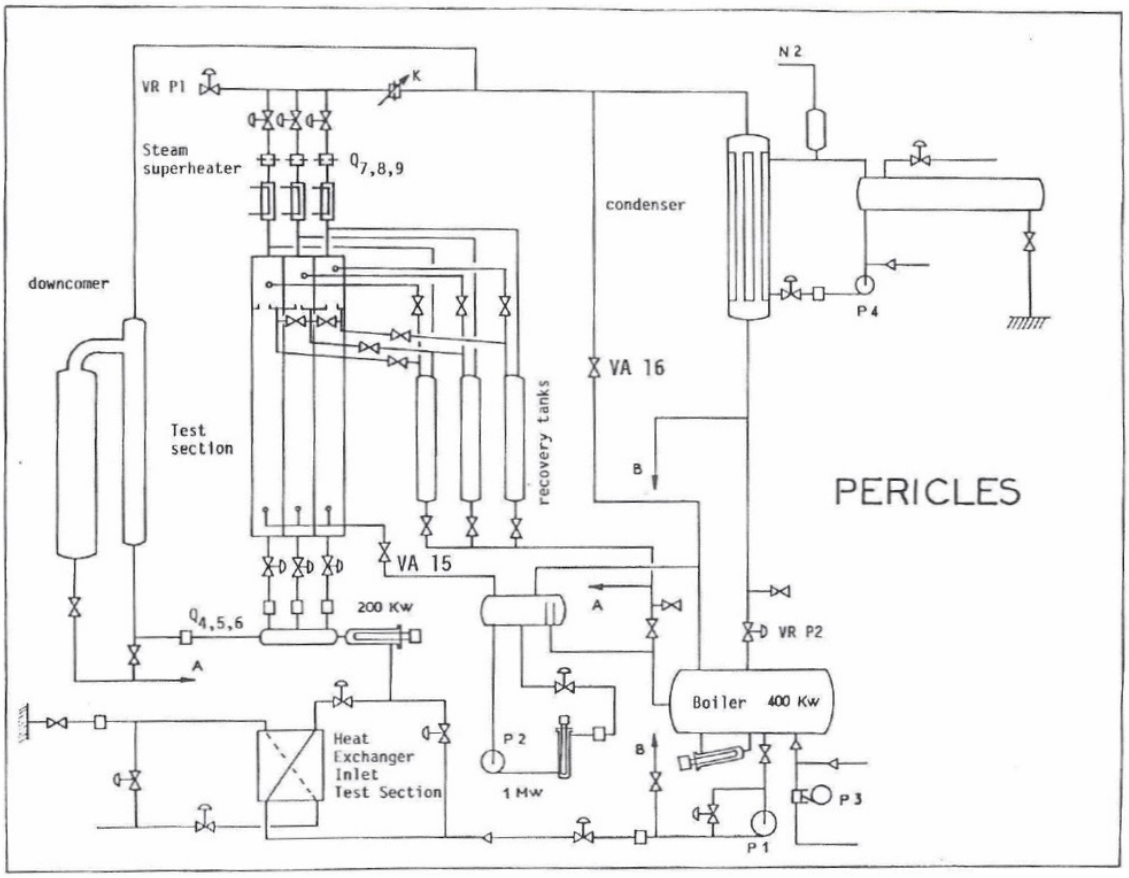

Figure 24: *A diagram of the PERICLES 2D facility with the test section consisting of three 7-by-17 assemblies side by side on the left.* [20]

The test section of the facility consists of a 3.656 m long 7-by-51 heated rod bundle divided into three 17 rod wide sections, referred to as assemblies hereafter. The rods can be electrically heated with two separate circuits allowing the middle assembly (hot assembly) to be heated with a higher power level than the two lateral assemblies (cold assemblies). Water is input from below with separate lines to each assembly. Above the test section the water outflow can be separated for each assembly, or be allowed to mix to permit water to flow back to different assemblies. In the experiments used in the PREMIUM benchmark the water outflow is separated for each bundle so as to not allow back flow.

The 9.45 mm diameter rods are made of boron nitride, with Nichrome V wires embedded inside to provide the heating, and clad in stainless steel. A cross section of the rods can be seen in Figure 25. The Nichrome V wire circles the center of the rod with the density of the circling varying in eleven steps to provide a cosine power profile shown also in Figure 25s. Due to the amount of Nichrome V varying throughout the length of the rods while the radius and the amount of the other substances is kept constant, the properties of the materials also vary accordingly.

Eight Framatome standard spacer grids align the rods in their place. Seven of the grids are situated inside the test section. The casing that houses the 357 rods is

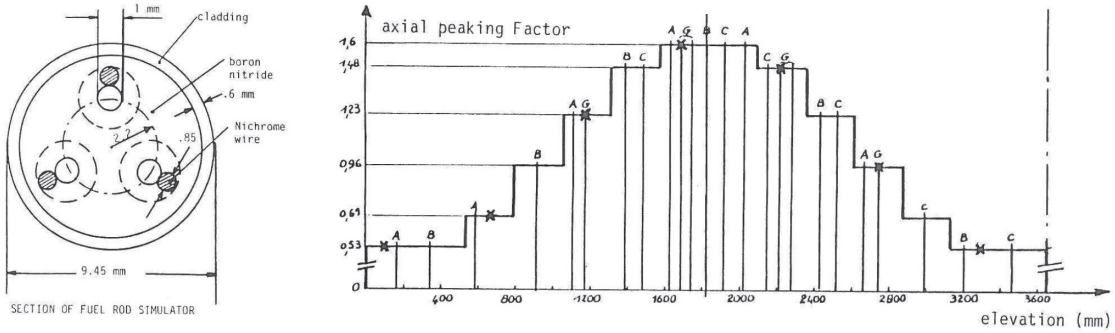

Figure 25: *A cross section diagram of the heater rods used in the PERICLES 2D facility (left) and axial peaking factors inside the rods (right).* [20]

made out of 7 mm thick stainless steel. The inner measures of the casing are 646.5 mm by 91.5 mm. It is heated with a tracing element to minimize its effect on the transient; the temperature is kept constant at a few degrees celsius over saturation to avoid condensation.

3.4.2 Experiments

Two different kinds of experiments were to be simulated with APROS for the PREMIUM benchmark Phase IV: boil-off experiments with level swell position and reflooding experiments with constant water inflow. Data for one boil-off experiment was provided for validating the model before calculating the reflooding experiments. No data of the reflooding experiments, other than initial cladding temperatures from one of them, was provided.

The boil-off experiments were performed by filling the test section to a certain point, turning the power on and then adjusting the inlet water flow while keeping the collapsed water level approximately the same. The rods gradually heated up until a steady state was found after which the inlet water flow, pressure losses and cladding temperatures were recorded.

In the reflooding experiments the power was turned on and the rods were allowed to heat until the maximum cladding temperature reached a set point. At this point water was let in to the steam filled channel. A quench front subsequently propagated through the channel filling it with water and cooling the rods.

3.4.3 APROS model of the facility

When designing the APROS model of the PERICLES 2D facility simplicity was an important goal due to the complex nature of the two dimensional phenomena. For this reason only the test section and a few additional nodes above and below it were modeled. The size of the heat structure and thermal hydraulic nodes was selected to match that of the FEBA model while accommodating the geometrical restrictions, mainly the eleven different axial power regimes. The housing was chosen to not be modeled because of its role in the experiments was only to eliminate heat losses. A picture of the model is portrayed in Figure 26.

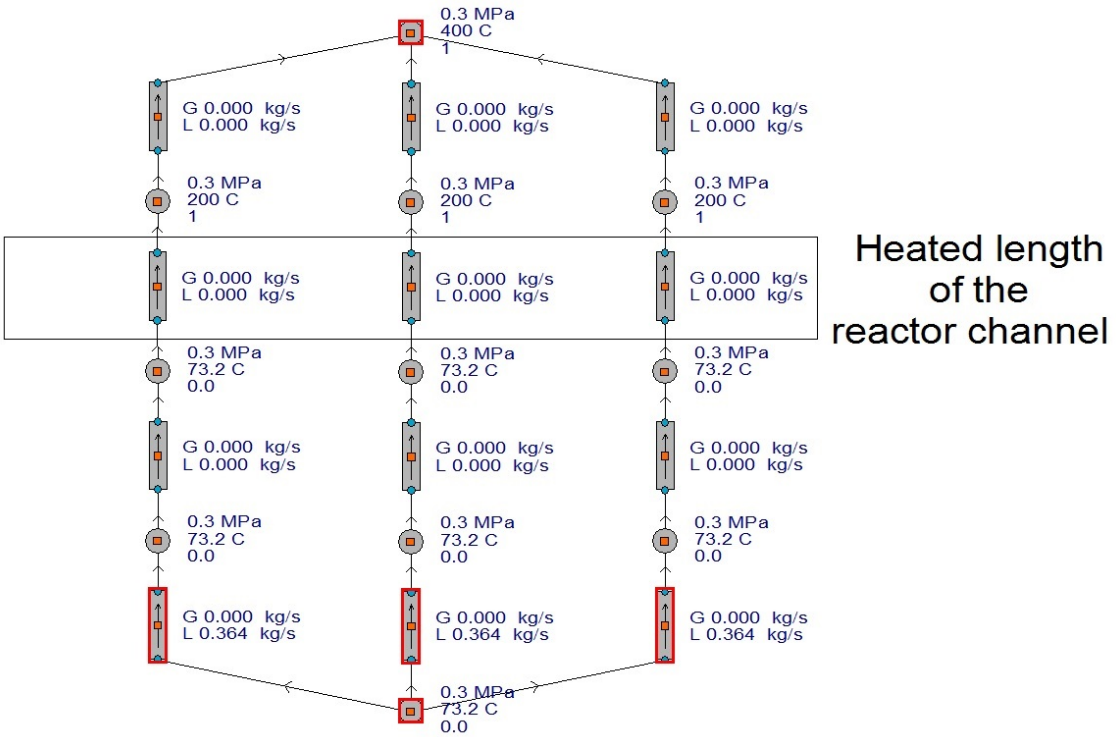

Figure 26: *The APROS model of the PERICLES 2D facility.*

The reactor channel depicted by the PERICLES 2D facility was divided in the APROS model into three pipe elements. The pipes were divided into 84 axial nodes, as were the rods also. Each thermal hydraulic node was connected to one heat structure node on the surface of the rods with a heat transfer module. The thermal hydraulic nodes were also connected to each other with thermal hydraulic branches from center to center according to their placement in the channel to create the two dimensional effect. A form loss coefficient of 9.02 was applied based on the equation of Idel'Chik [21] as adopted in the PREMIUM Phase IV specifications [22].

Radially the rods are divided into ten nodes allowing for nine layers. The first three layers, with an outer radius of 2 mm, are boron nitride followed by a 0.4 mm thick layer of Nichrome V. Then another three layers of boron nitride with a total thickness of 1.75 mm cover the Nichrome V. The final two layers with a thickness of 0.575 mm consist the stainless steel cladding. The layer structure was chosen in this manner due to recommendations from *Commissariat à l'énergie atomique et aux énergies alternatives* (CEA) based on their own modeling with CATHARE thermal hydraulic system code [22].

3.4.4 Validation of the APROS model

Data of one boil-off experiment performed with the PERICLES 2D facility was provided to validate each PREMIUM benchmark participants simulation model. This was enacted by comparing the results of the experiment when calculated with the APROS model of the facility to the experimental results. The most important

parameters of the experiment are described in Table 11 for the experimental and calculated cases.

Table 11: *The most important parameters of the test number BO0002. Experimental and calculated results are shown.* Φ_{nom} *refers to the average heat flow on the surface of the heater rods, HA and CA refer to hot and cold assemblies,* Φ_{xy} *defines the hot assembly power multiplier, GO is the inlet water flow, DT is the inlet water subcooling and P is pressure at the top of the test section.*

Test No	$\mathbf{\Phi_{nom}}$ **(HA)** **(W/cm²)**	$\mathbf{\Phi_{nom}}$ **(CA)** **(W/cm²)**	$\mathbf{\Phi_{xy}}$	**GO** **(g/cm²s)**	**DT** **(°C)**	**P** **(bar)**	**Swell level (m)**	**Collapsed level (m)**
BO0002 exp	2.7	2.7	1	1.067	60	3	2.74	1.33
BO0002 calc	2.7	2.7	1	1.17	60	3	2.74	1.22

Table 11 shows that the collapsed water level was approximately 10 % lower in the simulation than in the experiment. The inlet water flow, on the other hand, was approximately 10 % higher. Figure 27 presents the cladding temperatures and pressures along the width of the channel. The experimental data has been provided by the PREMIUM benchmark phase IV organizer, CEA.

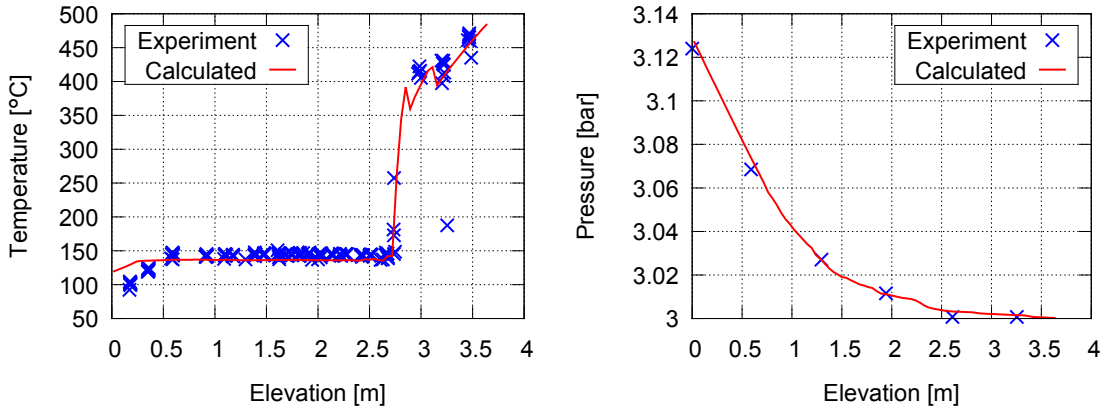

Figure 27: *Comparison of the test number BO0002 experimental and calculated temperatures and pressures along the width of the channel in the middle assembly.*

Both output parameters follow the experimental results very precisely. In the case of the cladding temperatures in the bottom of the test section there is a difference between calculated and experimental results. It is caused by the correlation used to calculate heat transfer in laminar flow having been defined in higher flow velocities. The influence on the general results of the calculation is minuscule due to the fact that in the affected region the flow is still fully liquid.

The swell level, or the point where stable film boiling starts and cladding temperatures rise rapidly, was set to be approximately 2.74 m by adjusting the inlet

flow. In this sense it is to be expected that the calculated values are close to the experimental ones. The height of the water column in the bubbly flow boiling region, however, is defined mainly by interfacial friction; the stronger the friction between vapor and liquid, the higher the vapor is able to carry the liquid. From this in turn it follows that by adjusting interfacial friction in bubbly flow the collapsed water level can be matched to the experimental settings. For example with input parameter *interfacial friction bubbly* set to 0.5 instead of 1, while the inlet flow and swell level are at the same values of 1.17 m and 2.74 m, the collapsed level sets at 1.31 m.

Interfacial friction in bubbly flow was found not to be influential in reflooding during the second phase of the PREMIUM benchmark. Since by adjusting the inlet flow the APROS simulation model is able to produce a pressure profile and cladding temperatures matching experimental values, including after onset of film boiling, it can be said that the model is validated and can be used to calculate the reflooding experiments required in the Phase IV of the benchmark.

3.4.5 Initial reflooding results

Six reflooding experiments performed at the PERICLES 2D facility are to be simulated for the PREMIUM benchmark. Due to the fact that the experimental data is not available at the time of writing only results for one experiment, test number RE0062, are analyzed. The list of specifications for all the six experiments are shown in Table 12.

Table 12: *The most important parameters of the reflooding tests.* Φ_{nom} *refers to the average heat flow on the surface of the heater rods, HA and CA refer to hot and cold assemblies,* Φ_{xy} *defines the hot assembly power multiplier, GO is the inlet water flow, DT is the inlet water subcooling, P is pressure at the top of the test section and* T_{wi} *is the initial cladding temperatures at the middle of the hot and cold assemblies.*

Test No	$\mathbf{\Phi_{nom}}$ **(HA)** **(W/cm²)**	$\mathbf{\Phi_{nom}}$ **(CA)** **(W/cm²)**	$\mathbf{\Phi_{xy}}$	**GO** **(g/cm²s)**	**DT** **(°C)**	**P** **(bar)**	$\mathbf{T_{wi}}$ **(HA)** **(°C)**	$\mathbf{T_{wi}}$ **(CA)** **(°C)**
RE0062	2.93	2.93	1	3.6	60	3	600	600
RE0064	4.2	2.93	1.435	3.6	60	3	600	475
RE0069	2.93	2.93	1	3.6	60	3	475	475
RE0079	4.2	2.93	1.435	3.6	90	3	600	475
RE0080	4.2	2.93	1.435	5	60	3	600	475
RE0086	4.2	2.93	1.435	3.6	60	4	600	475

The output parameters required for the Phase IV are time trends of cladding temperatures at elevations 1.828 m and 2.998 m, as well as middle pressure drop between elevations 1.296 m and 1.942 m. Additionally, the maximum cladding temperatures and quenching times are to be extracted from the aforementioned cladding time trends.

Initial BEPU calculation of the reflooding experiment with test number RE0062 were performed. 93 runs were simulated for 1000 seconds using simple random sampling of the input parameters defined in Table 10 according to their respective

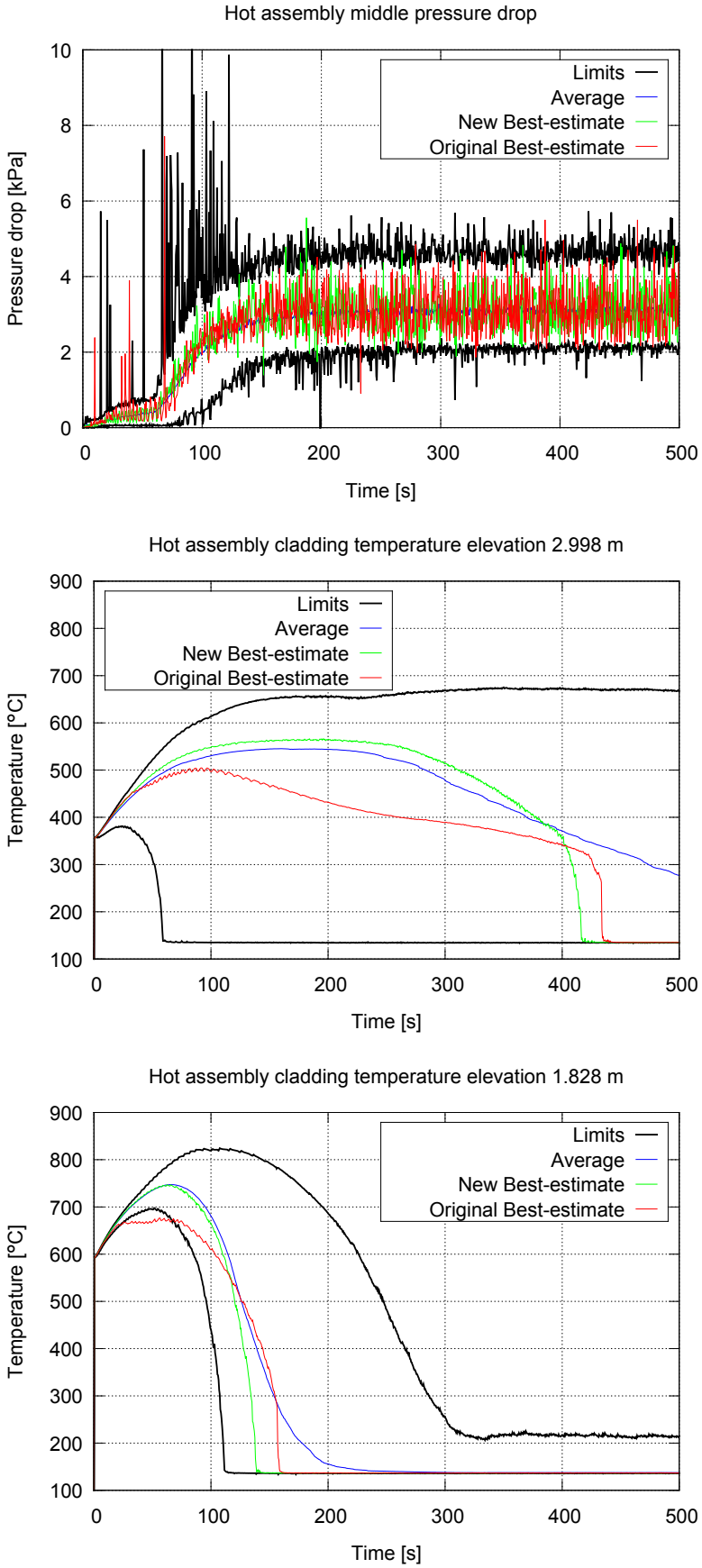

Figure 28: *PERICLES 2D reflooding test number RE0062 initial BEPU calculation results for three selected parameters.*

PDFs. The results for the time trends required in the PREMIUM benchmark Phase IV are presented in Figure 28 along with their 95 %/95 % minimum and maximum limits. The scalar values extracted from the time trends are respectively presented in Table 13.

Table 13: *Scalar value results of the initial BEPU run of PERICLES 2D reflooding test number RE0062. Two different ways of extracting the quench times have been used: extracting from the quench front elevation trend calculated by APROS and the time when cladding temperature drops below 250 °C. For the quench times X means that no quenching occurred at that elevation during the 1000 seconds of operation*

Point	**Old Ref**	**New Ref**	**Min**	**Max**
Maximum cladding temperature 1.828 m	677	747	699	824
Maximum cladding temperature 2.998 m	504	566	383	675
Quench time 1.828 m (quench front elevation)	159	139	112	X
Quench time 1.828 m (cladding time trend)	157	135.5	109.5	301
Quench time 2.998 m (quench front elevation)	435	417.5	248	X
Quench time 2.998 m (cladding time trend)	429.5	412	50	X

The most notable characteristic of the results is that the minimum and maximum limits give very wide bounds for the cladding temperatures. The possibility exists that the rods do not fully quench, as demonstrated by the cladding temperature at 2.998 m staying at a level near 700 °C. On a closer examination of the single run results it is apparent that this scenario is not a likely one and is, in fact, produced in only maximum of two runs; at the 1000 second mark, which was the last recorded time in the simulations, in 7 cases the rods have not quenched, but 5 or 6 of these appear to be on the path to quenching based on quench front propagation trend.

Similarly it can be noted that the lower limit of quenching, when deducted from the cladding temperature time trend, is earlier in the higher point. This means that in some cases the rods quench first in both ends while a section of the rods in the middle still has not quenched. Also, the quench time deducted from the quench front elevation is much larger for this point, because it is essentially the time when the rods quench fully. Since the average values in the time trend are close compared to the calibrated values it is evident that not many runs show this kind of behavior. In fact, when comparing quenching times for all of the runs it is found out that only 2 runs out of the 93 runs act in this manner.

In one other case the quench times derived with the two different approaches disagree: the quench time upper limit for 1.828 m. The discrepancy arises from the different ways of deducting the quench front elevation and that in the particular

run, which is the one run that does not appear to be on the path to quenching, the quench front sets at approximately that elevation.

Another point that can be made of the results is that the reference calculation run with the old, nominal values of the input parameters is set inside the bounding curves for the most part. The only exception is the highest cladding temperatures, but this is similar to the FEBA calculations, where the original best-estimate calculation produced lower maximum cladding temperatures and slightly later quench times.

3.5 Findings

The Post-BEMUSE REflood Models Input Uncertainty Methods benchmark consists of identifying influential input parameters for reflooding situations in thermal-hydraulic system codes, defining the uncertainties related to them and, moreover, verifying that the definitions have been correctly formulated by carrying out a validation phase. The identification in the case of VTT participation with APROS, for the most part, was presented in a previous report [18] with some additional work showcased in the previous sections. The most important phase in the benchmark, Phase III, in which the uncertainties were defined, was also demonstrated in the previous sections along with an introduction to the last phase, verification.

After a bug was found in the calculation of entrainment and the FEBA calculation results were changed to a degree a new round of identification of the influential parameters was performed. Along with some additional judgment calls the list of parameters was shrunk from 10 to 6. These parameters were then subjected to three different methods for solving their uncertainties in the form of probability distribution functions.

The random variation application provided valuable information about the sensitivities of the output parameters to the input parameters and the relationships between the input parameters. It failed on the other hand to provide a direct result of the distributions of the parameters.

Both the FFTBM and the CIRCE methods proved to not be directly applicable to the situation at hand; the complexity of the problem with six influential parameters, some of them with large biases, was not solvable with one method alone. Thus a combination of the two was employed, with additional knowledge from the random variation runs also used.

The large biases in the correlations relating to reflooding manifest themselves through drastic differences between the APROS simulation results and experimental results. It would appear that not only are there biases in the correlations, but that the biases are not only related to the magnitude of the phenomena, which the correlations depict. This is evident in the excessively wide ranges of the PDFs defined for the input parameters, which are multipliers of the correlations. For example in the case of the parameter *Heat transfer to dry wall/Forced convection to gas*, which is essentially a one phase flow correlation, the range should be much smaller than the analysis provides.

The large uncertainties pertained to the input parameters also show in the initial BEPU results of the PERICLES 2D reflooding experiment RE0062. Even without

the experimental data it can be said that the bounding ranges for the cladding temperatures are excessively wide. It can be pointed out, though, that the maximum cladding temperatures are contained even while the possibility exists that the rods will not quench fully. Further calculations of the other PERICLES 2D tests will most likely shed more light on the consistency of this finding.

The PDFs of the input parameters are a result of the process based on code calculations, which was detailed previously. For this reason to achieve smaller ranges both the process as well as the reference calculation of the code need to be improved upon. As it stands, with the process described beforehand, using the FEBA experimental data, the distributions are as is. Further work to improve the correlations used by APROS to calculate reflooding, especially to eliminate the biases that are known to exist in the code, could greatly reduce the ranges of the distributions set for the input parameters.

4 Conclusions and discussion

The topic of this master's thesis was the quantification of uncertainties pertaining to the physical models of the thermal hydraulic system code APROS developed by VTT in collaboration with Fortum. The need for this arises from the trend in nuclear power plant safety research of accounting for uncertainties when performing analyses.

The most common approach to the so called Best Estimate Plus Uncertainty (BEPU) methodologies is the propagation of input uncertainties through code runs to produce lower and upper uncertainty limits of the outputs. The confidence of the limits is set with the amount of runs based on order statistics. For physical input parameters such as reactor core power, the uncertainties can be defined directly from the physical reality, while for the uncertainties relating to the way a code models the thermal hydraulic phenomena the code output must be compared to experimental results to deduct uncertainties in the modeling.

In the case of complex phenomena, such as those taking place during reflooding of a reactor core after a Loss Of Coolant Accident (LOCA), simple sensitivity analysis with one parameter will not suffice. Moreover, a standardized method for producing quantitatively comparable results for different parameters is required to avoid the ambiguity related to engineering judgment.

Three methods presented in the OECD/NEA/CSNI endorced Post-BEMUSE REflood Models Input Uncertainty Methods (PREMIUM) benchmark, which VTT is taking part in, were reviewed in this master's thesis. Two of them, the *Methodology for characterizing the range of input uncertainty parameters by the use of the FFTBM* (FFTBM) and the *Calcul des Incertitudes Relatives aux Corrélations Élementaires* (CIRCE), were used in a simple paradigm application, the FRIGG loop boiling water reactor experiments, to test their applicability with APROS. The third one, a method developed at the Karlsruhe Institute of Technology (KIT), was only briefly introduced because it resembles CIRCE, but is more complex. No ready software to use the method exists either, unlike in the case of CIRCE.

Due to issues with the data acquired from the FRIGG loop experiments, as well as possible issues with APROS correlations, the results of the uncertainty quantification were mixed; although the findings of the two methods supported each other, they did not provide conclusive, usable information. The ranges of the uncertainties were very wide and additionally envelope calculations utilizing the ranges did not cover all experimental values. Still, the conclusion was that the methods could be used with APROS and for that reason called for further investigation.

The next step was to apply the methods to the case presented in the PREMIUM benchmark, the FEBA reflooding experiments. In a previous study the parameters that were influential in reflooding had been identified. The list was further modified based on repeated analysis after fixing a bug in the code as well as removing parameters that were directly related to each other in the code.

In addition to the methods used on the FRIGG loop experiments to define the parameter uncertainties a crude method was explored. It consisted of running thousands of simulations with randomly selected parameter values to find out which

combinations would produce results close to the experimental ones. The method was found out to be too resource expensive to fully see through, although it gave valuable insights into the relationships of the parameters.

Neither the CIRCE nor the FFTBM methods were able to properly handle the analysis of the six chosen parameters, of which some had biases. CIRCE most likely failed due to the complexity of having six variable parameters and FFTBM was not able to find the biases of several parameters. CIRCE, on the other hand, seemed to be able to do this. Thus, first the biases were distinguished with the help of CIRCE, and then FFTBM was used to find the ranges of the uncertainties.

An immediate observation of the uncertainty ranges identified for the parameters was that they were very large. Further work into finding the optimal mean values for the parameters could have had an impact on the broadness of the definitions, but the possible improvements were not seen to be worthwhile taking into account the resources required and the time frame of the PREMIUM benchmark. Moreover, this suggested that the biases troubling APROS were not simply a matter of magnitude.

Another approach into improving the precision of the uncertainties associated to the parameters would be to fully repeat the analysis starting with the simulation model of the FEBA facility built with APROS. Yet, even then, the issues with the correlations of APROS relating to reflooding would exist and would burden the results. Also, the CIRCE and FFTBM methods would still be limited in their usefulness.

In addition to the problems with CIRCE and FFTBM already discussed, a method that could take into account parameter uncertainties that are previously known would be of great use. For example physical parameter uncertainties or parameters that can be assigned a distribution based on single effect test. This functionality could most likely be implemented into the French method CIRCE, or to the German method KIT, but would require extensive work both on the theoretical part as well as on the software development part.

The fourth phase of the PREMIUM benchmark, the verification of the definitions of the uncertainties is underway and VTT contribution to it was introduced with the PERICLES 2D facility. The preliminary results suggested, as was expected, that the parameter probability distributions were excessively wide. On the other hand the peak cladding temperatures in the reflooding experiment analyzed were limited to a reasonable degree. Also, without the experimental data of the PERICLES 2D tests no conclusive attestation of the quality of the results can be made.

Significant issues exist in the definition of the uncertainties of the physical models of APROS. Yet the probability distribution functions, as wide as they are, can be considered as the present knowledge of the uncertainty related to them; they are wide for a reason.

Future work is required to be able to use BEPU methodologies with APROS in safety analyses. More experiments must be used to evaluate the uncertainties existing in APROS. The optimal scenario would be to use all the experiments that are a part of APROS validation and verification to define and validate the uncertainties. This is especially important for reflooding experiments, because of the complex nature of the phenomena taking place in them.

The methods used for the quantification of the uncertainties in APROS should also be studied further and, if possible, refined. Here the continuance of international co-operation is crucial. Although the uncertainties of the correlations themselves can not be derived from international work due to code specific differences, the methods used for the quantification are not dependent on the codes.

The result of the work presented in this master's thesis are probability distribution functions of input parameters that are for most parts so wide that their information content is limited. Additionally some of them are not in accordance with current standard use of APROS due to the large biases and the ranges not covering the nominal values. However, the findings are of great value and work as a basis for both code improvement as well as further studies into refining the use of BEPU methods with APROS.

References

[1] A. Prošek and B. Mavko. "Review of Best Estimate Plus Uncertainty Methods of Thermal-Hydraulic Safety Analysis". In: International Conference: Nuclear Energy for New Europe 2003. Nuclear Society of Slovenia. 2003.

[2] *Best estimate safety analysis for nuclear power plants: uncertainty evaluation.* Safety reports series 52. STI/PUB/1306. Vienna: International Atomic Energy Agency, Aug. 2008. ISBN: ISBN 9789201089076.

[3] A. Bucalossi et al. "Comparison Between Best-Estimate-Plus-Uncertainty Methods and Conservative Tools for Nuclear Power Plant Licensing". In: *Nuclear Technology* 172.1 (Oct. 2010), pp. 29–47.

[4] *Report of a CSNI workshop on uncertainty analysis methods (1994 : London, England).* NEA/CSNI/R(1994)20. Nuclear Energy Agency, Aug. 1994.

[5] *Report on the Uncertainty Methods Study.* NEA/CSNI/R(1997)35. Nuclear Energy Agency, June 1998.

[6] *BEMUSE Phase V Report: Uncertainty and Sensitivity Analysis of a LB-LOCA in ZION Nuclear Power Plant.* NEA/CSNI/R(2009)13. Nuclear Energy Agency, Dec. 2009.

[7] F. D'Auria and W. Giannotti. "Development of a Code with the Capability of Internal Assessment of Uncertainty". In: *Nuclear Technology* 131.2 (Jan. 2000), pp. 159–196.

[8] H. Glaeser. "GRS Method for Uncertainty and Sensitivity Evaluation of Code Results and Applications". In: *Science and Technology of Nuclear Installations* 2008 (Feb. 2008). Article ID 798901.

[9] S. S. Wilks. "Determination of Sample Sizes for Setting Tolerance Limits". In: *Ann. Math. Statist.* 12.1 (1941). Princeton University, pp. 91–96.

[10] A. Petruzzi and F. D'Auria. "Approaches, Relevant Topics, and Internal Method for Uncertainty Evaluation in Predictions of Thermal-Hydraulic System Codes". In: *Science and Technology of Nuclear Installations* 2008 (Oct. 2007). Article ID 325071.

[11] C. E. Shannon. "Communication in the presence of noise". In: *Proceedings of the Institute of Radio Engineers* 37.1 (1949), pp. 10–21.

[12] A. de Crécy. "Determination of the Uncertainties of the Constitutive Relationships in the CATHARE 2 Code". In: International Conference on Mathematical Methods to Nuclear Applications M&C. Salt Lake City, Utah, USA. Sept. 2001.

[13] D. G. Cacuci. "Sensitivity and Uncertainty Analysis of Models and Data". In: *Nuclear Computational Science.* Springer Netherlands, 2010. Chap. 6, pp. 291–353.

[14] Y. L. G. Celeux A. Grimaud and E. de Rocquigny. "Identifying Intrinsic Variability in Multivariate Systems Through Linearized Inverse Methods". In: *Inverse Problems in Science and Engineering* 18.3 (Jan. 2010), pp. 401–415.

[15] D. G. Cacuci and M. Ionescu-Bujor. "Best–Estimate Model Calibration and Prediction Through Experimental Data Assimilation – I: Mathematical Framework". In: *Nuclear Science and Engineering* 165.1 (May 2010), pp. 18–44.

[16] A. Petruzzi, D. G. Cacuci, and F. D'Auria. "Best–Estimate Model Calibration and Prediction Through Experimental Data Assimilation – II: Application to a Blowdown Benchmark Experiment". In: *Nuclear Science and Engineering* 165.1 (May 2010), pp. 45–100.

[17] O. Nylund et al. *Hydrodynamic and Heat Transfer Measurements on a Full–Scale Simulated 36–Rod Marviken Fuel Element with Uniform Heat Flux Distribution*. FRIGG Loop Project 2. R4–447/RTL–1007. Sweden: Ab Atomenergi and ASEA, 1968.

[18] T. Alku. *Identification of Influential Uncertain Parameters of PREMIUM Benchmark*. VTT-R-08026-12. VTT, Nov. 2012.

[19] T. Skorek. *Description of FEBA Test Facility and FEBA/SEFLEX Experimental Program*. GRS, 2012.

[20] R. Deruaz, P. Clement, and J. Veteau. *Study of Two-dimensional Effects in the Core of a Light Water Reactor During the ECCS Phase Following a Loss of Coolant Accident*. Commission of the European Communities, 1985.

[21] I. E. Idel'Chik. *Handbook of Hydraulic Resistance*. Translated from Russian - Israel Program for Scientific Translations, Jerusalem 1966. Moskva-Leningrad: Gosudarstvennoe Energeticheskoe Izdatel'stvo, 1960.

[22] A. de Crécy, P. Bazin, and J. Baccou. *PREMIUM: specifications for the phase IV using the 2-D reflooding PERICLES tests*. CEA, 2013.